Journal of Building Engineering 59 (2022) 105039

Contents lists available at ScienceDirect

Journal of Building Engineering

journal homepage: www.elsevier.com/locate/jobe

Improvement in the petrophysical properties of solid bricks by adding household glass waste

Laura Crespo-López *, Giuseppe Cultrone

Department of Mineralogy and Petrology, Faculty of Sciences, University of Granada. Avda. Fuentenueva s/n, 18002, Granada, Spain

ARTICLE INFO

Keywords:
Solid bricks
Household glass
Mineralogy
Petrophysical properties
Manufacturing processes
Compactness

ABSTRACT

The extensive consumption of clayey soils to manufacture bricks has caused the depletion of these non-renewable natural resources. In this paper, in a bid to reduce clay consumption and recycle waste glass, 20 wt% crushed household glass was added to clayey soils from Jun and Guadix (Granada, Spain) to manufacture handmade and extruded bricks fired at 800, 950 and 1100 °C. The presence of carbonates in the soil from Jun favored the development of new Ca-(Mg) silicates such as gehlenite, diopside, wollastonite and anorthite, while mullite developed in the bricks made with clay from Guadix. The addition of glass altered the porous system of the bricks, which absorbed less water and dried more quickly than conventional bricks. As regards the manufacturing procedure, extruded bricks turned out to be less porous than handmade ones. The porosity of both handmade and extruded bricks fell as the firing temperature increased. Bricks with added glass were more resistant to compressive strength tests than those made exclusively with clay. These results were confirmed by ultrasound measurements from which we observed that the compactness of bricks increases in line with the increase in the firing temperature and by adding glass. Accelerated ageing tests (freeze-thaw, salt crystallization and wet-dry) revealed that the addition of glass provides the bricks with more compactness, strength and durability than those without glass fired at the same temperature. 20 wt% proved to be the ideal proportion for waste glass added to the clay used in the production of high-quality compact bricks.

1. Introduction

Bricks are the most common ceramic products and are widely used in both historic and modern buildings [1]. Together with stone and concrete, they are amongst the most frequently used materials in construction. Unfortunately, in the last 20 years the market for these products within the construction industry has reached saturation point [2–5]. This has led the brick industry to diversify towards less standard, more competitive products [6]. In addition, the extensive consumption of clayey soils to manufacture bricks has caused the depletion of these non-renewable natural resources [7]. If we could replace at least part of these soils with other (preferably cheap) products, large savings could be made in raw materials, which together with the use of waste products, can generate a direct benefit for the environment. Therefore, the use of waste products as an additional material in brick manufacture could provide a solution to this problem [7–10]. It could also help reduce the accumulation of waste in landfills.

The waste products that could potentially be used in this way include household glass, an inert, amorphous, nonporous, fragile material [11] that has been part of our lives for thousands of years [12]. Much of the common bottle glass produced is difficult to

* Corresponding author.
E-mail addresses: lcrespo.geo@gmail.com, lauracrespo9@correo.ugr.es (L. Crespo-López).

https://doi.org/10.1016/j.jobe.2022.105039
Received 6 May 2022; Received in revised form 11 July 2022; Accepted 23 July 2022
Available online 4 August 2022

recycle due to the colouring additives and lead content and may therefore end up in landfills. As an additive for bricks, the glass acts as a flux due to its Na_2O content and amorphous composition, which reduces the temperature required for brick sintering [9,13]. Although recycling waste glass for the production of new glass products has many advantages in terms of the conservation of raw materials, a considerable amount of this waste cannot be recycled and is dumped into landfills, producing pollution due to lead accumulation [14–16]. In this regard, the European Union generates around 0.9 million tons of waste glass each year (https://ec.europa.eu/eurostat/) and, according to the Environmental Protection Agency (EPA, https://www.epa.ie/), glass represents 5.1% of the total solid waste collected. Therefore, the use of household glass waste as an additive in brick manufacture could provide a way to "store" this waste product, so reducing landfill and the associated environmental burden.

The first research into the possible use of glass in brick manufacture was conducted in the 1970's. In these initial investigations varying amounts of between 5 and 94 wt% of glass was added [13,17,18 and references therein]. The conclusion was that the ideal amount of glass to add to the clay mixture was between 15 and 30 wt%. The effects of using this waste as an additive in brick production were further explored by Loryuenyong et al. [19], Kazmi et al. [20], Saenz et al. [21] and Hasan et al. [22], who studied the effects of added glass on the physical properties of bricks obtaining promising results, such as a decrease in porosity or an increase in compactness compared to other added wastes. Other authors added waste glass in brick production in an attempt to immobilize heavy metals [23] or to improve the intrinsic material properties and environmental development from the production of bricks with electroplating sludge [24]. In this study, we investigate a novel aspect of bricks made with added waste glass by comparing handmade and extruded samples from a petrophysical point of view. The most commonly used brick production method today is extrusion, which has advantages in terms of the speed of manufacture and the homogeneity of the final product. Nevertheless, in handmade brick production, it is easier to control the number actually required by the market, so reducing the consumption of raw materials [3,4,7,12]. This is why in this research we considered both manufacturing processes (handmade and extrusion) and analysed samples of both types of brick. To this end, crushed household glass was added to two clayey materials with a different mineralogical composition so as to assess how this waste product affects the petrophysical properties and durability of the bricks. Samples were made at three different firing temperatures in order to find out how the bond between the waste and the clayey matrix is affected by temperature.

2. Materials and methods

2.1. Preparation of the brick samples

Solid bricks were made using raw materials quarried in Guadix and Jun (both in Andalusia, Spain). Both raw materials are post-orogenic continental sediments deposited in the intermontane basins of Guadix-Baza and Granada. The raw material from Guadix was deposited in the middle-late Pleistocene during the last stages of the infilling of the basin [25,26], above all in small lakes and swamps that developed temporarily on the banks of braided rivers that drained from the nearby Sierra Nevada mountains [26]. The raw material from Jun was deposited during the late Turolian in a lacustrine environment with nearby fan deltas that drained carbonate sediments eroded from Sierra Arana [27].

The extruded and handmade bricks used in this research were made with the raw materials (from Guadix or Jun) plus 20 wt% household glass waste. These were then compared with handmade samples made without glass, which served as the control group (Table 1). As regards the decision as to how much waste should be added to the bricks, Dondi et al. [28] demonstrated that the addition of up to 2 wt% glass did not produce any significant change in the fired ceramics, but with 5 wt% glass addition, an improvement in mechanical properties was observed. Phonphuak et al. [29] found that the addition of up to 10 wt% glass enhanced the physical properties of the bricks. The decision to add a larger quantity of waste, i.e. 20 wt%, was based on recent investigations which seemed to show that this resulted in better performance [13,16–20]. It was also a way of reusing more waste. Household glass was milled into powder before being mixed with the raw materials, so as to increase its specific surface area and improve possible reactivity with the brick matrix.

Extruded bricks made with clay from Guadix and Jun were provided by the brick factory that supplied the two raw materials (Cerámica Castillo Siles, S.L., Víznar, Spain). The extruded bricks measured approximatively 1 × 2 × 5 cm.

As for the handmade bricks, the raw materials were sieved and fragments of over 1.5 mm in size were discarded. They were then mixed with the glass (when applicable) and with water. 308 ml/kg and 333 ml/kg of kneading water were required to knead the raw materials from Guadix and Jun, respectively. Once enough plasticity had been achieved, the clayey paste was placed in moistened wooden moulds of 15 × 20 × 4 cm. After 1 h, the moulds were removed and the clayey pastes were cut into 4 cm edge cubes using a stretched cotton thread and left to dry.

Table 1
Acronyms assigned to the bricks according to the raw material used, the addition of 20 wt% household glass, the production process and the firing temperature.

Raw material	Production process			Firing temperature (°C)
	Handmade	Handmade + glass	Extrusion + glass	
Jun (J) and Guadix (G)	J800	Jg800	Jge800	800
	G800	Gg800	Gge800	
	J950	Jg950	Jge950	950
	G950	Gg950	Gge950	
	J1100	Jg1100	Jge1100	1100
	G1100	Gg1100	Gge1100	

Once the extruded and handmade samples were dry, they were fired in a Herotec CR-35 electric oven at 800 °C, 950 °C and 1100 °C. The temperature inside the oven was initially kept constant for 1 h at 100 °C so as to eliminate any residual moisture in the samples. Then, the temperature was increased at a rate of 2 °C/min. Once the desired temperature was reached, the oven was kept at a constant temperature for 3 h. Finally, it was turned off and the samples were left to cool slowly. They were not removed from the oven until the next day. Slow cooling prevents the development of fissures due to β-to-α quartz transition. After removal from the oven, the bricks were immersed in water for about 1 h so as to prevent possible "lime blowing" due to the presence of lime grains [30]. Glass bubbles with a diameter of up to 1 mm developed in the bricks made with the clay from Guadix and fired at 1100 °C (samples Gg1100 and Gge1100, Table 1).

2.2. Analytical techniques

2.2.1. Chemistry, mineralogy and texture

The granulometry of the raw materials from Guadix and Jun and that of the household glass was measured using a Galai CIS-1 laser gauge. X-ray fluorescence (XRF) was used to determine the major elements in the two raw materials, the fired bricks and the household glass with a PANalytical Zetium compact spectrometer. 3 g of each sample was ground to powder prior to its analysis. The mineralogical composition of the raw samples, clay fraction and fired bricks was determined by powder X-ray diffraction (PXRD) using a PANalytical X'Pert PRO diffractometer. The working conditions were as follows: CuKα radiation, 45 kV voltage, 40 mA current, 3–70° 2θ exploration range, 0.1 2θ s^{-1} goniometer speed. The mineral phases were identified using the PANalytical X'pert Highscore Plus 3.0 software. As regards the clay fraction, the following oriented aggregates were prepared according to the recommendations of Moore and Reynolds [31]: air dried (OA), solvated with ethylene glycol (OA + EG), solvated with dimethyl sulfoxide (OA + DMSO) and heated at 550 °C (OA+550).

The thermal decomposition of the two raw materials up to 950 °C was determined by a thermogravimetric analysis coupled with differential scanning calorimetry (TG/DSC) using a METTLER-TOLEDO TGA/DSC1 apparatus. The petrographic features (mineralogy and texture) of the fired samples were observed by means of polarized optical microscopy (POM). Observations under plane- and cross-polarized light were carried out on polished thin sections using a Carl Zeiss Jenapol-U microscope equipped with a Nikon D7000 digital camera. Detailed observations of reaction rims among phases and of the development of sintering and vitrification of the matrix were performed on the same thin sections using a high-resolution field emission scanning electron microscope (FESEM) Carl Zeiss SMT (AURIGA series) coupled with energy dispersive X-ray analysis (EDS).

2.2.2. Determination of the pore system

Hydric and porosimetric tests were carried out in order to shed light on the pore system of the bricks. Free (Ab, at atmospheric pressure) and forced (Af, under vacuum) water absorption, drying (Di) and capillarity tests (C) were carried out according to UNE-EN 13755 [32], NORMAL 29/88 [33] and UNE-EN 1925 [34] standards, respectively. These tests enabled us to determine the degree of pore interconnectivity (A_x) [35], the saturation coefficient (S), the apparent (ρ_a) and real (ρ_r) densities and the open porosity (P_o) [36]. Hydric tests were performed under controlled thermo-hygrometric conditions (20 °C and 60% relative humidity) using deionized water. Three samples per brick group were analysed.

The pore system of the bricks within a range of 0.002–200 μm was analysed by mercury intrusion porosimetry (MIP) using a Micromeritics Autopore IV 9500 porosimeter. Open porosity (P_{oMIP}, %), specific surface area (SSA, m^2/g) and apparent and real densities (ρ_{aMIP} and ρ_{rMIP}, g/cm^3) were calculated.

2.2.3. Mechanical behaviour

The compressive strength (Rc) was measured using a Matest E181 hydraulic press with double frame 25 kN/300 kN according to the UNE-EN1926 [37] standard. This analysis was only carried out on the cubic-shaped handmade samples, as the extruded bricks had a different shape and did not fit into the press properly. Rc was calculated in MPa on three samples of each brick according to the following Eq. (1):

$$Rc = \frac{F}{A} \tag{1}$$

where F is the breaking load (in N) and A is the cross-sectional area in m^2.

2.2.4. Non-destructive testing

Ultrasound gives a measure of the degree of compactness and was used to determine the elastic-dynamic properties of the bricks, properties that affect their mechanical resistance. Measurements were performed using a Control 58-E4800 ultrasonic pulse velocity tester with transducers of 54 kHz and a circular surface of 27 mm in diameter. A water-based eco-gel was used to allow a homogeneous contact between the transducers and the brick. The measurements were carried out on three samples per brick type. P-wave propagation was measured in m/s according to the ASTM D2845 [38] standard. The structural anisotropy (ΔM) was also calculated using the following Eq. (2) [39]:

$$\Delta M = 1 - \frac{2VP_1}{VP_2 + VP_3} \cdot 100 \tag{2}$$

where V_{P1}, V_{P2} and V_{P3} are the propagation velocities of the P-waves in the three orthogonal directions.

Colour measurements were performed to quantify the lightness and chromaticity of the fired bricks. A Konica Minolta CM-700d

spectrophotometer was used following the UNE-EN 15886 [40] standard. Illuminant D65, 10° observer angle and 8 mm measurement area were used. Nine measurements per sample were performed. Once the lightness (L*) and chromatic values (a* and b*) had been determined, the total colour variation (ΔE) between bricks without additive and with added household glass was calculated as follows (Eq. (3)):

$$\Delta E = [(\Delta L^*)^2+(\Delta a^*)^2+(\Delta b^*)^2]^{(1/2)} \quad (3)$$

2.2.5. Accelerated ageing tests

Thirty freeze-thaw, fifteen salt crystallization and thirty wet-dry cycles were performed to observe a theoretical degradation that could affect the lifetime of the handmade and extruded bricks according to the UNE-EN 12371 [41], UNE-EN 12370 [42] and ASTM D 5313 [43] standards, respectively. The freeze-thaw test studies the fatigue caused in pores and fissures by the increase in the volume of water due to freezing at temperatures below 0 °C. The salt crystallization test reproduces the decay that the bricks may undergo due to the dissolution and recrystallization of soluble salts within their porous systems. The wet-dry test simulates the disintegrating and dissolving action of water when enhanced by temperature. Brick decay during these ageing tests was monitored daily by weighing the bricks and observing possible loss of fragments on their surface.

3. Results and discussion

3.1. Granulometry, chemistry and mineralogy of raw materials and waste

3.1.1. Grain size distribution

The granulometric analysis shows that the raw materials from Jun and Guadix have unimodal particle size distribution although they differ in terms of maximum peak size and curve shape (Fig. 1). While the Guadix curve is quite symmetric with a maximum at 25 μm, the Jun curve shows a maximum at 100 μm and has a marked asymmetry at lower granulometric values. The powdered glass shows three maxima at 7 μm, at around 40 μm and at 300 μm.

3.1.2. X-ray fluorescence (XRF)

Table 2 shows the chemistry of the two clayey samples and the household glass. The raw materials from Jun and Guadix have different compositions (Table 2). The presence of CaO (11.2%) and MgO (4.1%) in the clay from Jun is a sign of its carbonate content, while the clay from Guadix is carbonate-free (CaO is 0.6 and MgO is 0.9%). According to Maniatis and Tite [44], the raw material from Jun can be classified as calcareous, while the Guadix clay has higher SiO_2, Al_2O_3 and Fe_2O_3 contents.

The household glass is mainly composed of SiO_2 (71.7%), Na_2O (12.3%) and CaO (12.3%), i.e., the typical compounds of common glass: silica sand, calcium carbonate and sodium carbonate and can be classified as soda-lime glass [45]. The considerable amounts of Na_2O + K_2O (13.2%) and CaO + MgO (11.7%) in the household glass could act as an energetic fluxing agent in the production of ceramics [46,47]. In addition, the presence of alkali oxides ensures that the glass will have a low softening point during firing. This could help reduce the firing temperature of the bricks [48].

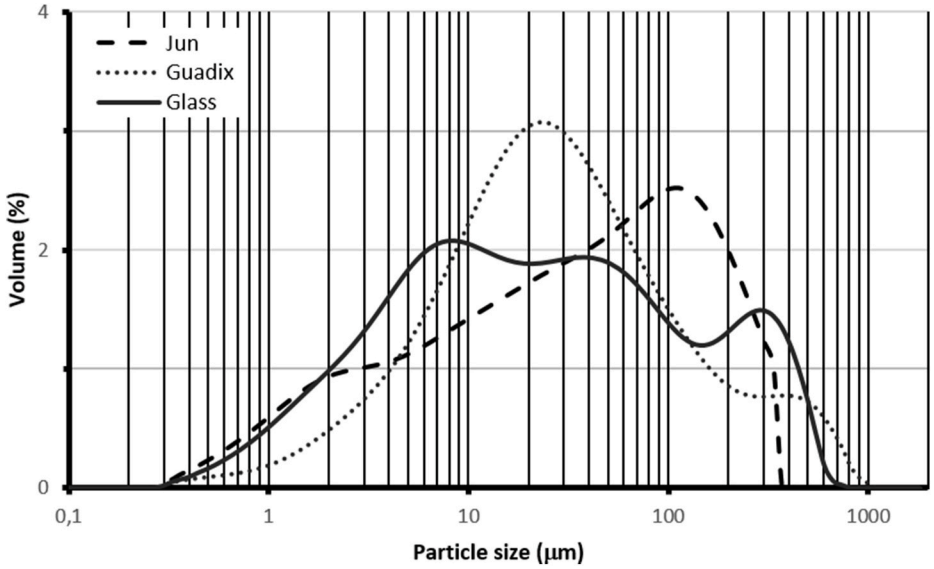

Fig. 1. Grain size distribution of the clayey raw materials from Jun and Guadix and of household glass.

Table 2
XRF (in %) results for the raw materials from Jun and Guadix and the household glass used to manufacture the bricks.

	SiO_2	Al_2O_3	Fe_2O_3	MnO	MgO	CaO	Na_2O	K_2O	TiO_2	P_2O_5	LOI	Total
Jun	44.63	14.76	5.21	0.06	4.10	11.28	0.84	2.84	0.72	0.12	15.19	99.75
Guadix	63.13	17.79	7.13	0.07	0.96	0.63	0.85	2.67	1.26	0.13	5.34	99.96
Glass	71.71	1.90	0.40	0.01	1.35	10.34	12.33	0.90	0.11	0.03	0.88	99.96

3.1.3. Powder X-ray diffraction (PXRD)

PXRD analysis reveals the presence of phyllosilicates (illite, paragonite, chlorite and kaolinite), quartz and k-feldspar (microcline) in the raw materials from Jun and Guadix (Fig. 2). Carbonates (calcite and dolomite) and hematite were only detected in the sample from Jun. The presence of chlorite, a mineral that is commonly masked by smectite and kaolinite, is revealed in the clay fraction of both samples by heating the OA at 550 °C [48]. The raw material from Jun has a slightly higher concentration of kaolinite, illite and paragonite than that from Guadix.

3.1.4. Thermogravimetry (TG-DSC)

TG-DSC analysis highlighted that at around 100 °C both raw materials suffer a slight weight loss due to the presence of moisture or hygroscopic water (Fig. 3). At 300 or 340 °C there is an inflection in the DSC curves, which corresponds to the combustion of labile organic matter present in the raw materials [50,51]. Other endothermic peaks, corresponding to the dehydroxylation of phyllosilicates, can be identified at about 540 °C [51–53]. Dehydroxylation of these minerals is complete at 600 °C [54] and therefore does not contribute significantly to the weight loss that takes place at higher temperatures. According to Velde [55], the equilibrium temperature for dehydroxylation of muscovite and its complete decomposition at 1 atm is approximately 560 °C. Therefore, as in other previous research [53,56,57], the dehydroxylation of the phyllosilicates in the raw materials from Jun and Guadix is not an equilibrium process.

The clay from Jun undergoes a much more pronounced weight loss, which is clearly visible in the TG curve with a minimum endothermic peak at around 800 °C and a 13% mass loss. This is due to the decomposition of carbonates and the release of CO_2 [18,56,58]. Above 800 °C, both samples show a further small weight loss, which is attributed to the further dehydroxylation of illite-type phyllosilicates [48,53,54,59]. The clay from Jun suffered a total weight loss of 16%, while the clay from Guadix lost 6%, values that were very similar to those measured by XRF (LOI, Table 2).

3.2. Chemistry, mineralogy and texture of the fired bricks

3.2.1. X-ray fluorescence (XRF)

Table 3 shows the chemistry of the fired bricks. They have the same chemistry as the raw materials. The only difference is the lower loss on ignition (LOI) values, given that the fired samples have lost any organic matter that may have been present in the raw material. The Jun samples have also lost almost all their carbonate content [58]. LOI values decrease as firing temperature increases due to the gradual dehydroxylation of phyllosilicates and, in the Jun samples, due to the decomposition of any remaining carbonates. LOI values are lower in bricks with added household glass because 20 wt% of the raw material is replaced by this additive. These samples are therefore less rich in phyllosilicates and carbonates.

3.2.2. Powder X-ray diffraction (PXRD)

All the phyllosilicates have disappeared in brick groups fired at 800 °C, with the exception of a dehydroxylated illite, although the reflection (001) at 10 Å is lower compared to that observed in the raw materials, suggesting that there is a lower concentration of this phase. The most abundant phase is quartz. As regards the presence of carbonates in Jun samples, at 800 °C dolomite has already disappeared while calcite content has fallen considerably (J800, Fig. 3). According to Rodríguez-Navarro et al. [60,61], dolomite starts to decompose at 500 °C and disappears completely at around 900 °C, while calcite starts to decompose at 600 °C and disappears completely at around 850 °C. At 800 °C, hematite starts to appear in the Guadix samples (G800, Fig. 4). At this temperature, the bricks with and without glass are mineralogically identical, although higher background noise can be observed in the samples with added glass due to the presence of this increasingly amorphous waste [62].

At 950 °C, the differences between the samples with and without glass are more pronounced than at 800 °C. In both brick groups, orthoclase transforms into a higher temperature polymorph phase, sanidine (Figs. 4 and 5). Hematite increases in concentration, mainly in Guadix samples, probably due to the decomposition of phyllosilicates, which favour Fe recrystallization [59]. In the Jun samples (Fig. 4) calcite has disappeared while new mineral phases - gehlenite, wollastonite and diopside - are detected. Rathossi and Pontikes [63] pointed out that gehlenite is formed by the reaction between illite, calcite and quartz. Wollastonite and diopside can be formed by the reaction between quartz and carbonates [64,65]. The addition of glass brings about further mineralogical changes in that it seems to act as a flux agent accelerating the reactions or increasing the formation of new mineral phases. This is evident for example in the fact that illite has disappeared in the Jg950 and Jge950 samples, while a new phase, anorthite, has appeared. These bricks also seem to have higher concentrations of gehlenite, wollastonite, diopside and hematite than J950. The samples from Guadix fired at 950 °C had a lower illite content than at 800 °C, but there was almost no difference in the mineralogy between the bricks made with and without glass (G950, Gg950 and Gge950, Fig. 5).

The mineralogical changes produced by the addition of glass become more obvious at 1100 °C (Figs. 4 and 5). In both brick groups (Jun and Guadix), there is an increase in the amorphous component, which suggests that the vitrification of the matrix is more advanced. The amount of hematite remains almost unchanged. In Jun bricks, the gehlenite content is lower in J1100 and disappears in

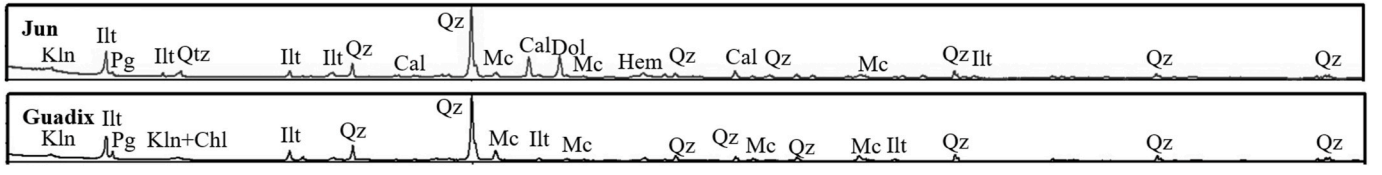

Fig. 2. X-ray diffraction patterns of the raw materials from Jun and Guadix. Legend according to Whitney and Evans [49]: Qz = quartz; Cal = calcite; Dol = dolomite; Ilt = illite; Pg = paragonite; Kln = kaolinite; Chl = chlorite; Hem = hematite; Mc = microcline.

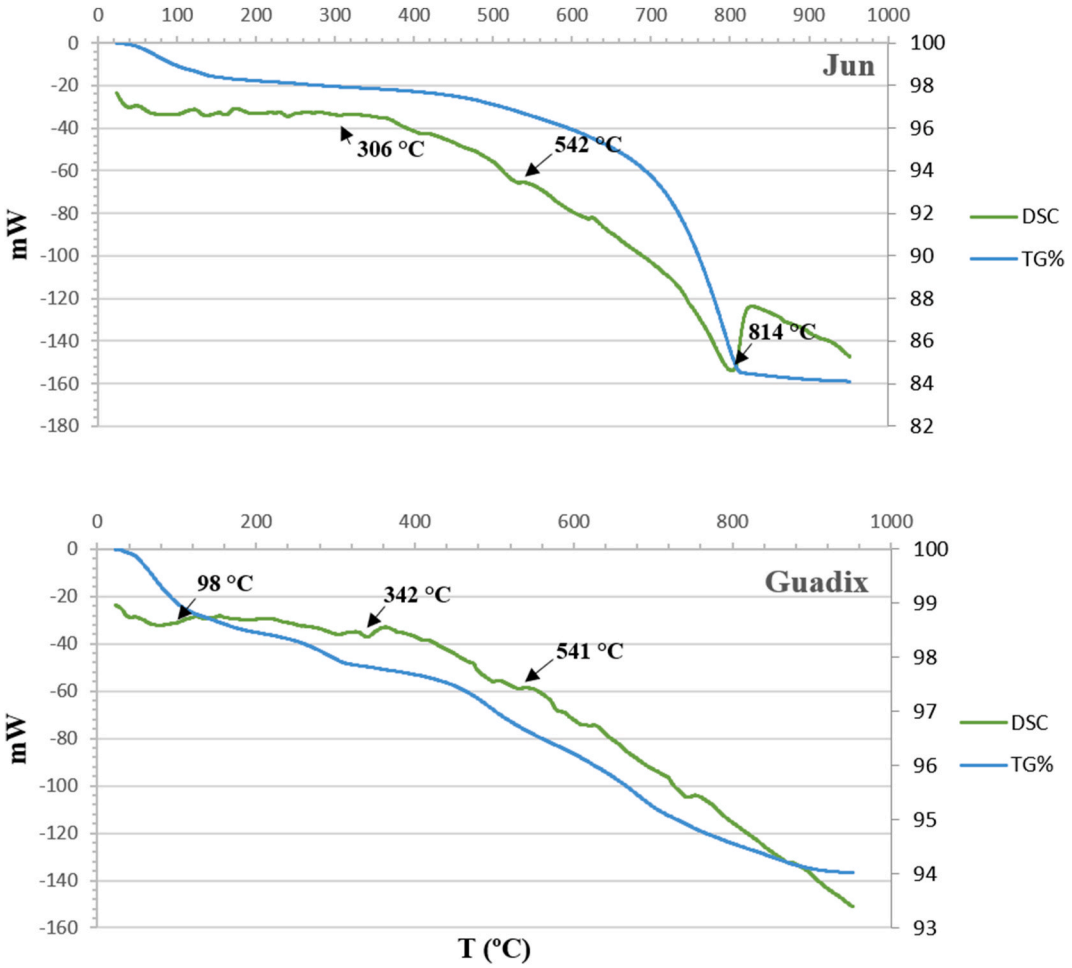

Fig. 3. TG-DSC analysis of the raw materials from Jun and Guadix. The abscissa represents the temperature (in °C) and the two ordinates represent the weight loss (in %) (TG blue curve) and the differential scanning calorimetry (in mW) (DSC green curve). (For interpretation of the references to colour in this figure legend, the reader is referred to the Web version of this article.)

Table 3
XRF results (in %) for the handmade and extruded (e) Jun bricks (J) and Guadix (G) bricks fired at 800, 950 and 1100 °C.

	SiO_2	Al_2O_3	Fe_2O_3	MnO	MgO	CaO	Na_2O	K_2O	TiO_2	P_2O_5	LOI	Total
J800	50.98	16.97	5.82	0.07	4.46	12.27	0.74	3.23	0.80	0.14	3.34	99.22
Jg800	56.27	13.49	4.58	0.06	3.63	11.86	3.40	2.68	0.65	0.11	2.75	99.48
Jge800	54.15	13.87	4.85	0.06	4.01	13.47	2.68	2.73	0.66	0.12	2.69	99.29
J950	52.86	17.40	5.92	0.07	4.33	12.20	0.77	3.31	0.81	0.14	1.65	99.46
Jg950	50.61	16.66	7.09	0.07	4.63	13.87	0.87	3.18	0.88	0.14	1.17	99.17
Jge950	54.91	14.01	4.93	0.06	4.09	13.86	2.71	2.74	0.65	0.12	1.10	99.18
J1100	55.13	14.52	6.54	0.09	3.58	11.83	3.14	2.86	0.75	0.12	0.82	99.38
Jg1100	54.38	13.75	6.67	0.07	3.55	12.51	3.74	2.91	0.80	0.11	0.84	99.33
Jge1100	52.94	13.83	6.67	0.07	4.07	13.93	3.27	2.91	0.80	0.12	0.57	99.13
G800	65.62	18.58	7.47	0.08	1.01	0.65	0.88	2.78	1.31	0.13	1.46	99.97
Gg800	66.37	15.14	5.92	0.06	0.96	2.80	3.32	2.37	1.01	0.11	1.92	99.98
Gge800	66.44	15.78	6.27	0.07	1.23	2.80	2.58	2.45	0.99	0.12	1.02	99.75
G950	65.86	18.89	7.54	0.08	1.01	0.64	0.89	2.83	1.28	0.14	0.83	99.99
Gg950	66.80	15.57	6.19	0.07	0.99	2.54	3.07	2.43	1.07	0.12	0.73	99.58
Gge950	66.25	15.84	6.30	0.06	1.20	2.89	2.61	2.47	1.01	0.12	0.68	99.43
G1100	65.86	18.82	7.61	0.08	1.03	0.66	0.90	2.81	1.30	0.13	0.41	99.61
Gg1100	66.26	15.58	6.25	0.07	1.17	2.83	3.31	2.42	0.96	0.12	1.01	99.98
Gge1100	66.61	15.91	6.40	0.07	1.43	2.82	2.61	2.47	1.00	0.12	0.51	99.95

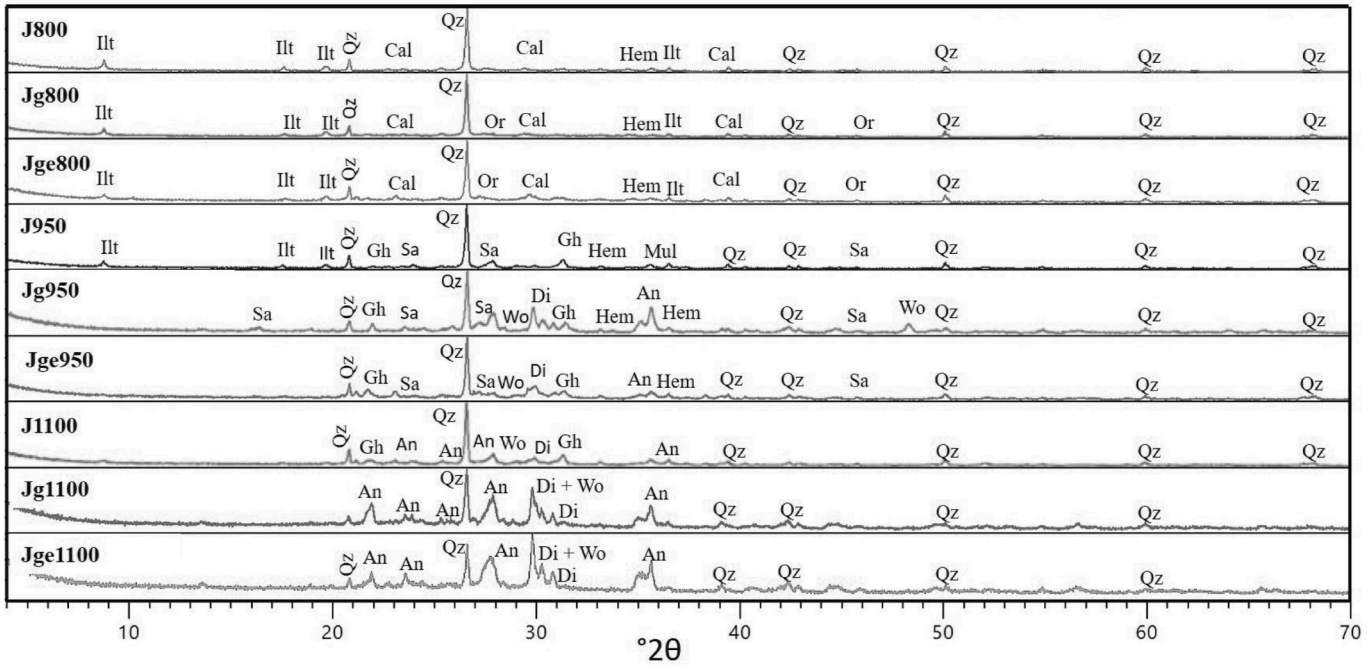

Fig. 4. X-ray diffraction patterns for bricks made with the raw material from Jun (by hand and by extrusion) and fired at 800, 950 and 1100 °C. Legend according to Whitney and Evans [49]: Qz = quartz; Cal = calcite; Ilt = illite; Hem = hematite; Or = orthoclase; Sa = sanidine; An = anorthite; Gh = gehlenite; Di = diopside; Wo = wollastonite.

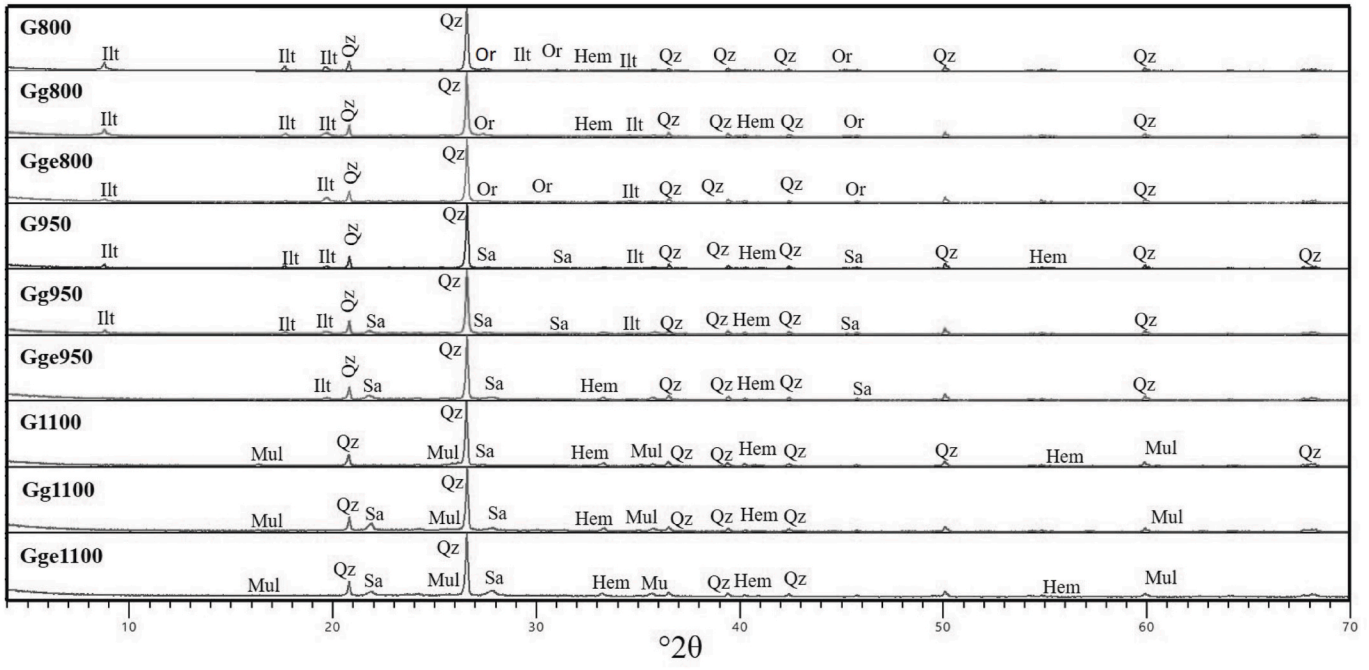

Fig. 5. X-ray diffraction patterns for bricks made with the raw material from Guadix (by hand and by extrusion) and fired at 800, 950 and 1100 °C. Legend according to Whitney and Evans [49]: Qz = quartz; Ilt = illite; Hem = hematite; Or = orthoclase; SA = sanidine; Mul = mullite.

Jg1100 and Jge1100 because it is involved in the formation of anorthite and wollastonite + diopside [64,65]. Another new phase, mullite, was identified in the Guadix bricks. According to Rodriguez Navarro et al. [66], this phase replaces the illite/muscovite inheriting specific crystallographic orientations of the phyllosilicate. The sanidine peaks are higher in the bricks with added glass.

3.2.3. Polarized optical microscopy (POM)

3.2.3.1. Jun. The observations under the microscope of the samples from Jun fired at 800 °C revealed the presence of fragments of metamorphic rocks (mica-schists and gneiss) of about 1 mm in length. These fragments are scattered in an orange matrix (Fig. 6A) that forms the main skeleton of the bricks. The carbonate grains are partially decomposed (Fig. 6B). For their part, the muscovite crystals appear unaltered and reach 2nd order interference colour. Phyllosilicates and elongated fragments often show a preferential orientation due to the pressure exerted on the raw material during kneading. This is also evident with the porosity as elongated pores follow the same orientation as planar minerals (Fig. 6C). Glass fragments start to decompose in Jg800, as manifested in the development of fan-shaped structures (Fig. 6D). At 950 °C, the matrix is slightly darker due to the gradual vitrification of the bricks [67]. The carbonates are completely decomposed and the phyllosilicates start to lose their birefringence, above all in bricks with added glass. At 1100 °C, due to the high firing temperature, the pores turn ellipsoidal-to-rounded in morphology and the matrix becomes dark (Fig. 6E). This phenomenon is again more noticeable in the samples made with glass (Fig. 6F), so confirming that the addition of glass accelerates textural changes.

3.2.3.2. Guadix. The bricks made with clay from Guadix fired at 800 °C (G800, Fig. 7A) have more quartz grains than those from Jun

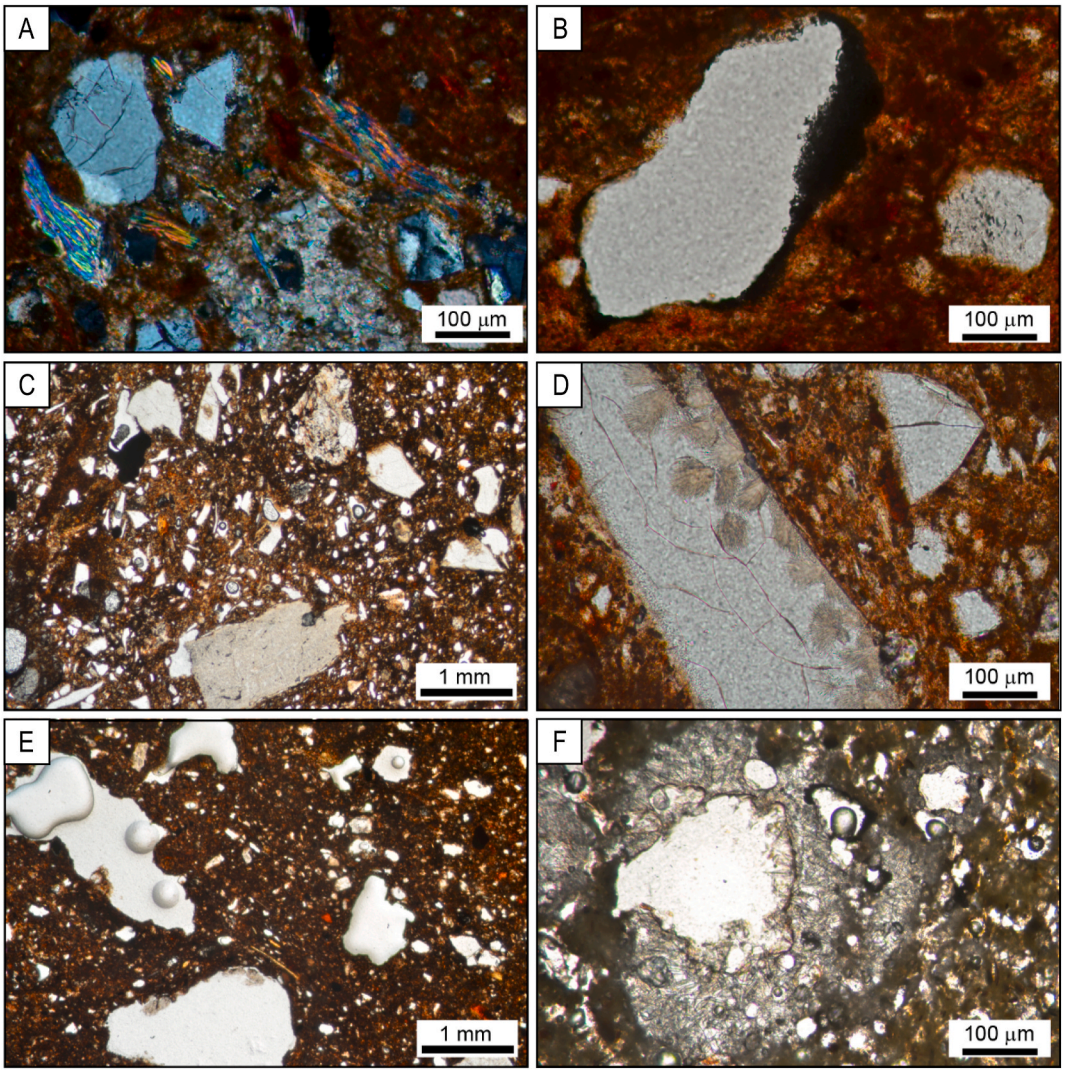

Fig. 6. Bricks made with clay from Jun with and without household glass fired at 800, 950 and 1100 °C. Abbreviation: PPL = plane-polarized light; PPX = cross-polarized light. A) fragments of quartz and gneiss fragments in the matrix of J800 (PPX); B) carbonate grain partially decomposed in J800 (PPX); C) general view of the matrix of Jg800 made with added glass (PPL); D) detailed image of a glass fragment in Jg800 which is starting to decompose (PPX); E) pores with different morphology in J950 (PPL); F) extended vitrification in the matrix of Jg1100 produced by the addition of glass (PPL).

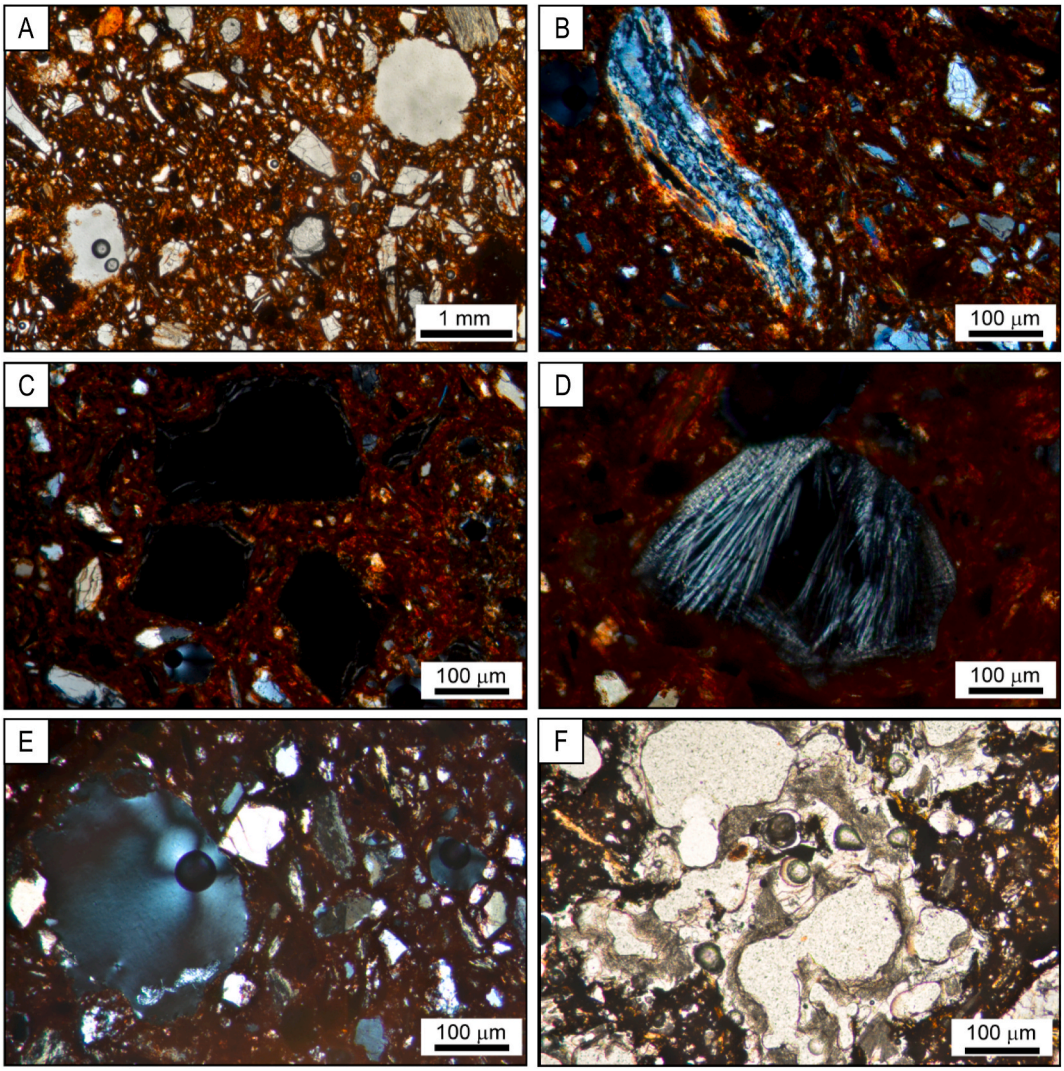

Fig. 7. Bricks made with clay from Guadix with and without household glass fired at 800, 950 and 1100 °C. Abbreviation: PPL = plane-polarized light; PPX = cross-polarized light. A) detailed image of the G800 sample showing fragments of quartz (PPX); B) matrix of Gg800 sample in which glass fragments with angular morphology are visible (PPX); C) glass fragments in the matrix of Gg800 sample (PPX); D) glass fragment in the Gg950 sample with acicular crystals intergrowth (PPX); E) detailed image of the matrix of the G1100 sample showing pores with varying shapes (PPX); F) porosity, melted glass and vitrification in the Gg1100 sample (PPX).

(Fig. 6C) and fragments of gneiss in an orange matrix (Fig. 7B). As in the Jun samples, phyllosilicates and elongated fragments (gneiss) often have a preferential orientation due to the pressure exerted during kneading. At 950 °C, the matrix becomes darker and the phyllosilicates become less birefringent. Glass fragments start to decompose in a similar way to that observed in Jun samples with the development of finger-type structures (Fig. 7C and D). At 1100 °C, muscovite-type phyllosilicates have lost their birefringence and have a whitish colour. According to Rodríguez Navarro et al. [66] and the PXRD results (Fig. 4), these phyllosilicates have probably been replaced by mullite. The pores acquire a rounded shape when the glass melts (Fig. 7F).

3.2.4. Field emission scanning electron microscopy (FESEM)

FESEM observations were only carried out on the bricks fired at 800 °C and 1100 °C, where any textural differences would be more significant (Fig. 8).

At 800 °C, in both brick groups the phyllosilicates maintain their laminar habit, although the lamellae tend to separate along the basal plane due to dehydroxylation (Fig. 8A) [65]. In the Jun bricks, the carbonate grains start to decompose, so confirming MOP observation. In some dolomite grains, a depletion of Ca at the core of these crystals could be observed (see EDS analysis in Fig. 8B). This is probably due to the higher mobility of Ca ions with respect to Mg, which gives rise to the formation of new phases such as gehlenite, so causing Ca content to fall. The addition of glass to the Jun bricks (Jg800) seems to favour the formation of reaction rims and the development of new phases. At 800 °C, a partial decomposition of glass fragments can be seen along the edge of these grains in the form of fan-shaped structures (Fig. 8C), as observed earlier under MOP (see Fig. 6D). These structures show depletion in Al and Na and a

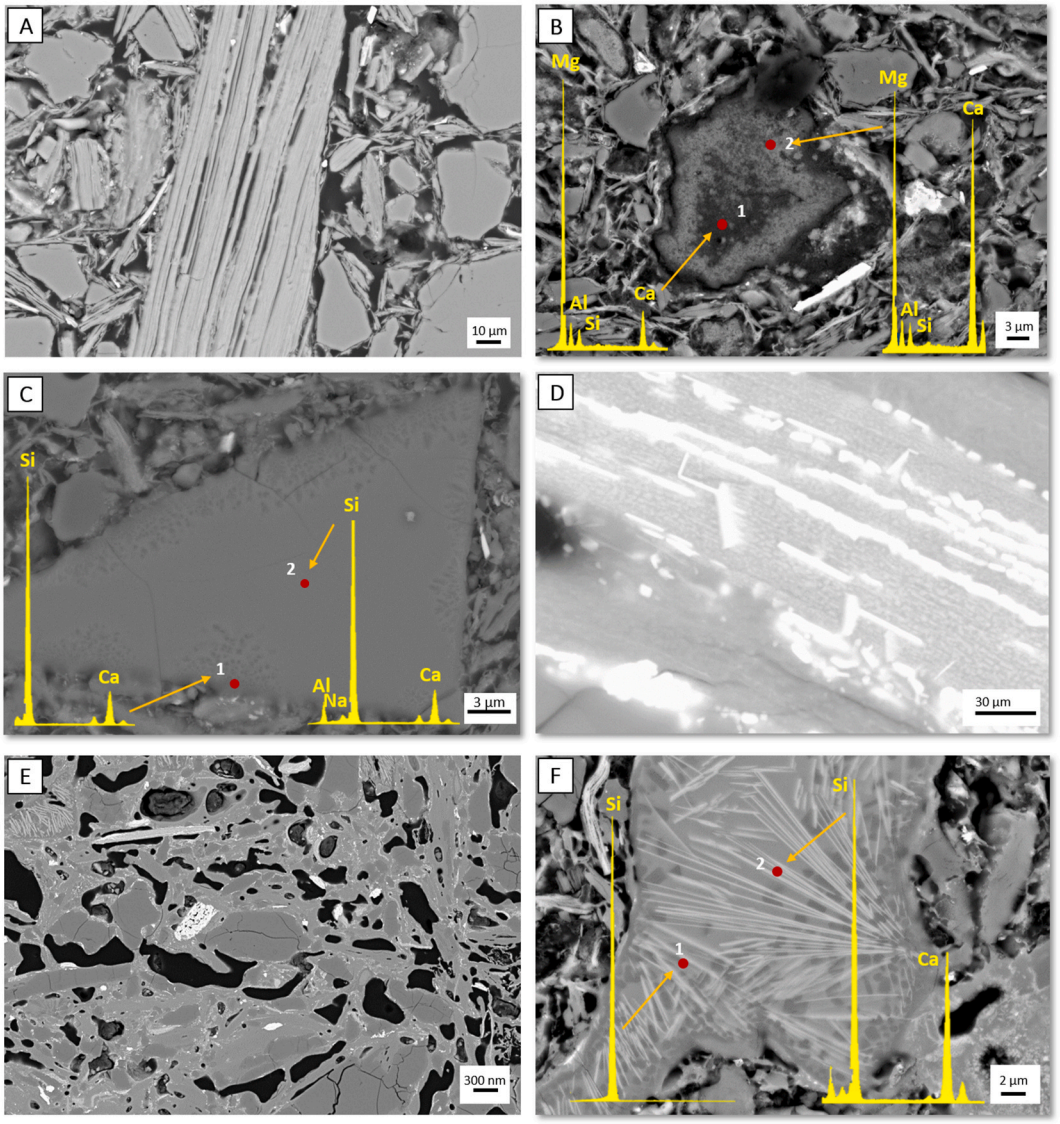

Fig. 8. A) Dehydroxylation of phyllosilicates along (001) planes in G800; B) view of J800 showing the partial decomposition of a dolomite grain with a depletion of Ca at the core; C) detail of a glass fragment from Jg800 showing the change in the composition along the edge of the grain due to devitrification or the formation of a pseudowollastonite; D) detail of small hematite crystal growth within the phyllosilicate sheets; E) rounded pores and small hematite crystals in Gg1100; F) detail of elongated crystals that have developed inside a glass fragment in Jg1100.

slight enrichment in Si. This could be due to an increase in β-wollastonite (pseudowollastonite), which forms at a lower temperature than α-wollastonite (wollastonite) [67–69]. Otherwise, these structures only indicate glass devitrification. Hematite crystals begin to nucleate in the matrix and within the phyllosilicate sheets (Fig. 8E). The addition of glass to the Guadix bricks fired at 800 °C (Gg800) does not accelerate the reactions between phases. At 1100 °C, the matrix of both brick groups was more vitrified and vitrification was more pronounced in the bricks made with glass. The pores become increasingly rounded and hematite crystals can be seen (Fig. 8D and E). The phyllosilicates lose their planar morphology and a secondary porosity can be detected inside these crystals. In the samples with added household glass (Gg1100 and Jg1100), the phyllosilicates have almost completely disappeared. Accessory minerals such as ilmenite and rutile have been identified. At this temperature, new phases such as gehlenite and diopside can be identified in the Jun bricks, and elongated crystals with a composition similar to that of wollastonite are clearly distinguishable inside the glass fragments (Fig. 8F). These findings confirm MOP observations and the data provided by PXRD results.

3.3. Hydric tests

The results of the absorption, drying and capillarity tests are shown in Table 4 and Figs. 9 and 10. In general, the behaviour of handmade and extruded bricks varies in line with the raw materials used and the presence or not of glass. All the samples absorb less water as firing temperature increases and with the addition of glass (Ab and Af, Table 4). Between the two groups, the Jun bricks

Table 4
Hydric parameters of handmade and extruded bricks. Ab: free water absorption (%); Af: forced water absorption (%); Ax: degree of pore interconnection (%); S: saturation coefficient (%); Di: drying index; P_o: open porosity (%); C: capillarity coefficient (g/m^2s^{05}); ρ_a: apparent density ($g\ cm^{-3}$); ρ_r: real density ($g\ cm^{-3}$).

	Ab	Af	Ax	S	Di	P_o	C	ρ_a	ρ_r
J800	27.32	27.43	0.40	85.39	1.08	40.96	3.09	1.96	3.23
Jg800	19.93	19.95	0.10	91.61	1.34	27.14	1.27	1.53	2.20
Jge800	22.65	26.97	16.02	93.20	1.39	25.64	0.57	1.17	2.37
J950	25.65	26.14	1.87	89.30	1.16	37.64	1.36	1.29	1.94
Jg950	21.52	25.80	16.59	81.23	1.47	26.48	1.06	1.48	2.39
Jge950	20.88	28.75	27,37	81.06	1.50	24.19	0.52	1.42	2.39
J1100	20.80	21.14	1.61	78.07	1.58	30.74	2.32	1.53	2.63
Jg1100	9.99	15.51	35.59	77.18	1.66	22.11	0.68	1.99	2.69
Jge1100	8.74	9.97	12.34	77.79	1.71	21.74	0.37	1.60	2.45
G800	21.44	21.75	1.43	86.25	0.91	39.24	3.26	1.69	2.68
Gg800	19.62	20.15	2.63	85.48	1.28	31.04	1.30	1.33	1.95
Gge800	20.95	22.18	5.55	74.35	1.30	30.27	0.36	1.55	2.62
G950	20.28	20.72	2.12	95.10	0.92	37.32	3.06	1.42	2.01
Gg900	17.59	18.92	7.03	79.71	1.34	24.15	1.09	1.59	2.28
Gge950	19.98	22.58	11.51	75.23	1.37	24.06	0.32	1.66	2.65
G1100	10.16	12.52	18.85	64.34	0.93	19.40	1.53	1.49	1.83
Gg1100	6.03	8.91	32.32	77.48	1.59	16.74	0.35	1.64	1.92
Gge1100	7.74	8.80	12.05	76.02	1.63	15.12	0.19	1.68	2.23

absorb more water than those from Guadix. The least absorbent of all were those made with glass and fired at 1100 °C (Gg1100 and Gge1100). The interconnection between the pores worsens (i.e., Ax values augment) as the firing temperature increases. This is because the gradual vitrification of the matrix worsens the interconnection between the pores [70], so making the bricks less absorbent (S, Table 4). As for the drying, the bricks fired at the lowest temperature dry faster (Di, Table 4), which is logical given that they have the best pore interconnection and water can flow out (i.e. dry) more easily. The Guadix bricks always dry faster than the Jun bricks (Figs. 9 and 10). The increase in the firing temperature (and the vitrification of samples) leads to a decrease in open porosity (P_o, Table 4). This decrease is more pronounced between 950 and 1100 °C, suggesting that the vitrification of the bricks occurs particularly in this firing range. It is interesting to note that the addition of household glass always reduces the porosity of the bricks, amongst which those manufactured by extrusion show the least porosity.

Water absorption by capillarity decreases as the temperature increases (C, Table 4). This tendency is accentuated by the addition of glass, above all, in extruded bricks.

As regards density, there is no clear tendency between the two groups and the firing temperatures. In general, the addition of glass seems to increase real density (ρ_r).

3.4. Mercury intrusion porosimetry (MIP)

The handmade Jun bricks (Fig. 11) with no added glass show a unimodal pore size distribution with a maximum peak at 0.4 μm (J800), 0.5 μm (J950) and 0.6 μm (J1100). This means that the increase in temperature causes larger maximum peaks. The addition of glass causes the maximum peak to shift to the right (towards larger pores) and leads to the formation of a second family of pores around 70 μm at 800 and 950 °C. At 1100 °C the curve turns trimodal with the appearance of two new families at around 1 and 100 μm (Fig. 11).

The Guadix samples (Fig. 12) follow the same trend as those from Jun, with a unimodal pore size distribution in the bricks without added glass and a maximum peak at 1 μm (G800), 1.9 μm (G950) and 2.1 μm (G1100). In the samples with added glass, a bimodal or polymodal distribution was detected. It is interesting to note that the specific surface area (SSA, in m^2/g, Figs. 11 and 12) generally drops as the firing temperature increases. This is due to the gradual coalescence of the smaller pores into larger ones at 950 and 1100 °C. If we compare bricks with and without the addition of household glass, the results show that those made with added glass have slightly lower SSA values at 800 °C, while significant drops are observed at 950 and 1100 °C. This suggests that the glass acts as a flux in the matrix of the bricks within this firing range (950–1100 °C).

3.5. Mechanical properties

The Jun bricks, with and without added glass, showed higher compressive strength than the Guadix bricks. The addition of glass always increases the strength (Table 5). This increase is related to textural and microstructural changes in the bricks. As mentioned before, glass acts as a flux agent bonding the particles together and reducing the porosity. The highest values were found in the bricks fired at 1100 °C, due to the high level of vitrification. The sample with the highest compressive strength (78.6 N/mm^2) was Jg1100.

Several authors have found that compressive strength is more closely related with porosity and the degree of vitrification than with the mineralogy of the clay [28,71–73]. Tite and Maniatis [74] found that in bricks made with carbonate-rich clays the structure formed at low temperatures (840–960 °C) remains almost unchanged until about 1080 °C. This is why Jun samples (without added glass) fired at 800 and 950 °C show very similar compressive strength. According to official specifications from the Spanish Ministry of Public Works (Pliego RL-88) [75], all the samples, with the exception of G800, have enough compressive strength to be used for construction purposes.

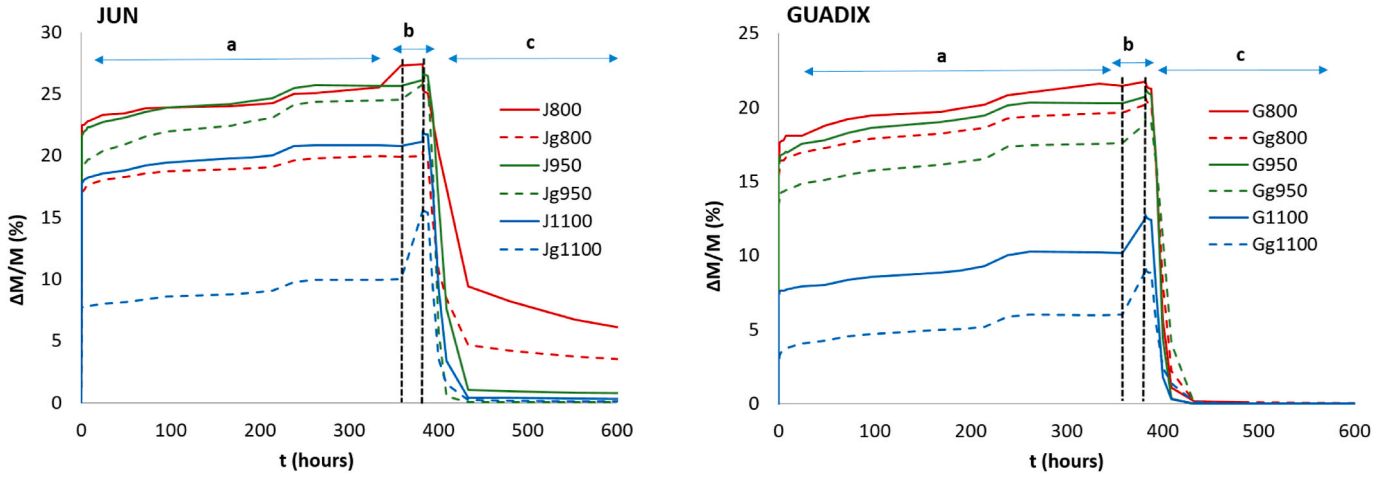

Fig. 9. Free (a) and forced water absorption (b) and drying curves (c) for handmade bricks made with and without household glass fired at 800, 950 and 1100 °C using the raw material from Jun and from Guadix.

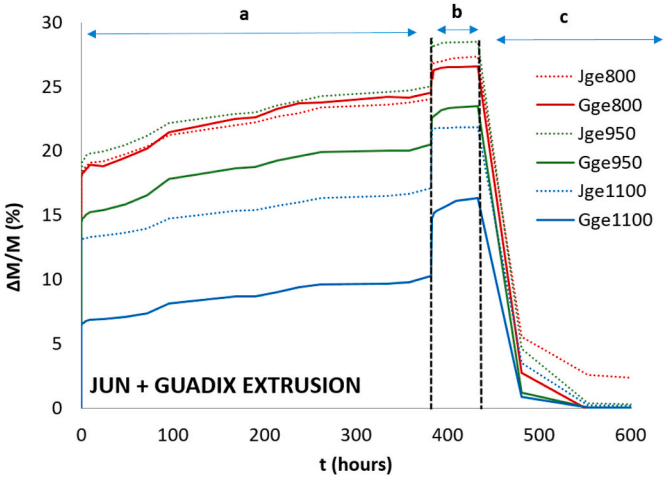

Fig. 10. Free (a) and forced water absorption (b) and drying curves (c) for extruded bricks made with household glass.

3.6. Ultrasounds

Fig. 13 shows the ultrasonic wave velocities propagation measured in handmade bricks with and without added glass. In general, the Jun bricks show higher Vp values than the Guadix bricks and the addition of glass tends to increase velocity values. This is because the bricks begin to vitrify and the internal structure becomes more homogeneous and loses the marked orientation provided by the phyllosilicates due to the addition of irregular, non-planar particles (glass). Ultrasound velocity increases not only with the addition of glass but also due to the increase in the firing temperature. It is interesting to note that the samples made with clay from Guadix show a gradual increase in velocity in line with increasing firing temperature, while those from Jun show similar values at 800 and 950 °C and a sharp increase at 1100 °C, especially in those made with added glass (Jg1100) This may be because the glass grains in the body of the brick cause the ultrasonic waves to scatter, so delaying their propagation [76,77]. The different behaviour between the two brick groups is due to their different mineralogical composition. In fact, even if the calcite and dolomite present in the raw material from Jun act as flux agents at low firing temperatures (800 °C), they do not promote vitrification at higher temperatures, in that the structure remains quite stable between 800 and 950 °C [72]. The formation of new Ca-(Mg-) silicate phases (gehlenite, wollastonite, diopside and anorthite) hinders the development of an alumina-silicate melt [74]. At 1100 °C the firing temperature is so high that both brick groups undergo extensive vitrification regardless of the composition of the raw material. Ultrasound tests indicate that as the firing temperature increases, bricks become more compact and tend to be more homogeneous as the structural anisotropy decreases [48].

3.7. Colour measurements

In Fig. 14, the bricks are grouped into three main groups based on their chromaticity. One group is made up of Jun bricks fired at 950 and 1100 °C with added glass (Jg950, Jge950, Jg1100 and Jge1100). These bricks have the lowest a* value and tend to be greyish/yellowish in colour. They also have the highest lightness values (L*, Table 6).

The second group is also made up of Jun bricks, mainly without added glass (J800, Jg800, J950 and J1100). The a* value is around 16 and the samples tend to be red/orange in colour. The third group is the largest. Most of the samples are made with the raw material from Guadix fired at different temperatures with and without added glass (Fig. 14). The a* value is over 19, and the samples have dark red tones, which is also because they have the lowest L* values (Table 6). The Guadix samples show a more reddish colour with higher a* and b* values than the Jun samples. This is due to the crystallization of iron oxides from the decomposition of Fe-containing minerals within illitic-chloritic clays, while in the Jun samples, Fe is partly involved in the formation of new Ca-silicates such as gehlenite [78,79]. On this question, Nodari et al. [80] observed that colour changes are related with the microstructural location and grain size of hematite particles as well as with the presence of iron in the glass rather than in the calcium silicate phases. This may explain why, as the firing temperature rises, the hematite content increases and a reddish colouration becomes more noticeable in the fired samples. Gg1100 bucks the general trend observed in the other samples (Fig. 14). This is due to the development of small glass bubbles on the surface (as described above in Section 2), which alter the colour values. In the Jun bricks, the samples that showed the greatest variation in colour due to the addition of glass were those fired at 950 °C, while the greatest variation in the Guadix bricks was observed in those fired at 1100 °C (ΔE, Table 6). According to Grossi et al. [81], colour variations of over 3 are perceptible to the human eye. This means that the variations in colour due to the addition of glass are visible in all the bricks except for those fired at the lowest temperature (800 °C).

3.8. Accelerated ageing tests

3.8.1. Freeze-thaw

All the bricks fired at 800 °C suffered more decay than those fired at higher temperatures, as might be expected given that they are less vitrified. The bricks fired at 1100 °C are generally the most resistant to ice and gain the least weight (Fig. 15). The addition of glass

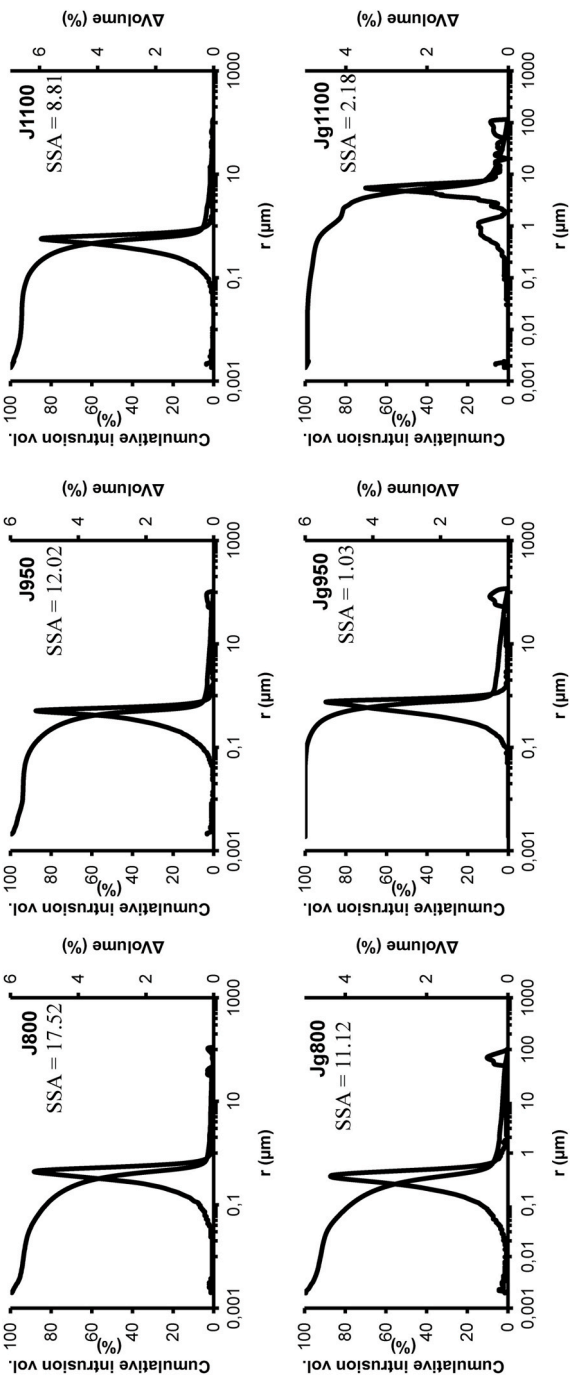

Fig. 11. MIP cumulative (dashed line) and pore size distribution (continuous line) curves for handmade bricks made with clay from Jun with and without added household glass fired at 800, 950 and 1100 °C.

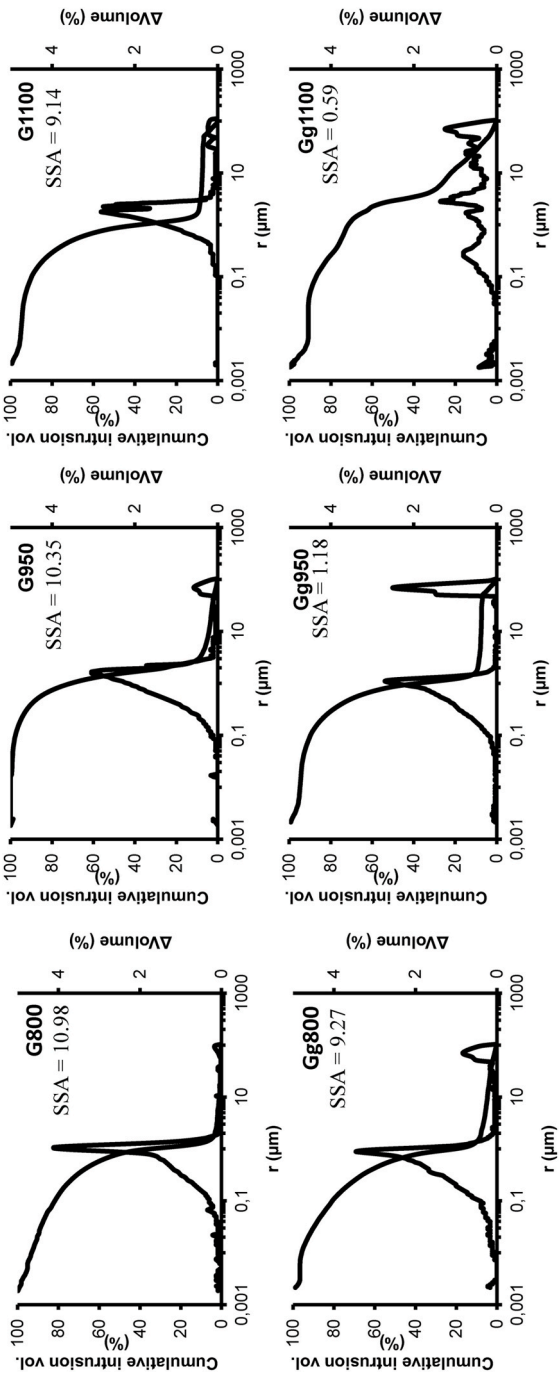

Fig. 12. MIP cumulative (dashed line) and pore size distribution (continuous line) curves for handmade bricks made with clay from Guadix with and without added household glass fired at 800, 950 and 1100 °C.

Table 5
Compressive strength (Rc, MPa) and standard deviation (σ) values for handmade bricks made with raw materials from Jun and Guadix with and without added glass.

	Rc	σ		Rc	σ
J800	21.8	0.7	G800	6.4	0.3
Jg800	33.2	1.8	Gg800	10.3	2.1
J950	24.4	1.1	G950	13.4	1.1
Jg950	36.8	2.0	Gg950	17.3	0.8
J1100	26.4	2.7	G1100	23.8	1.4
Jg1100	78.6	0.6	Gg1100	45.9	0.6

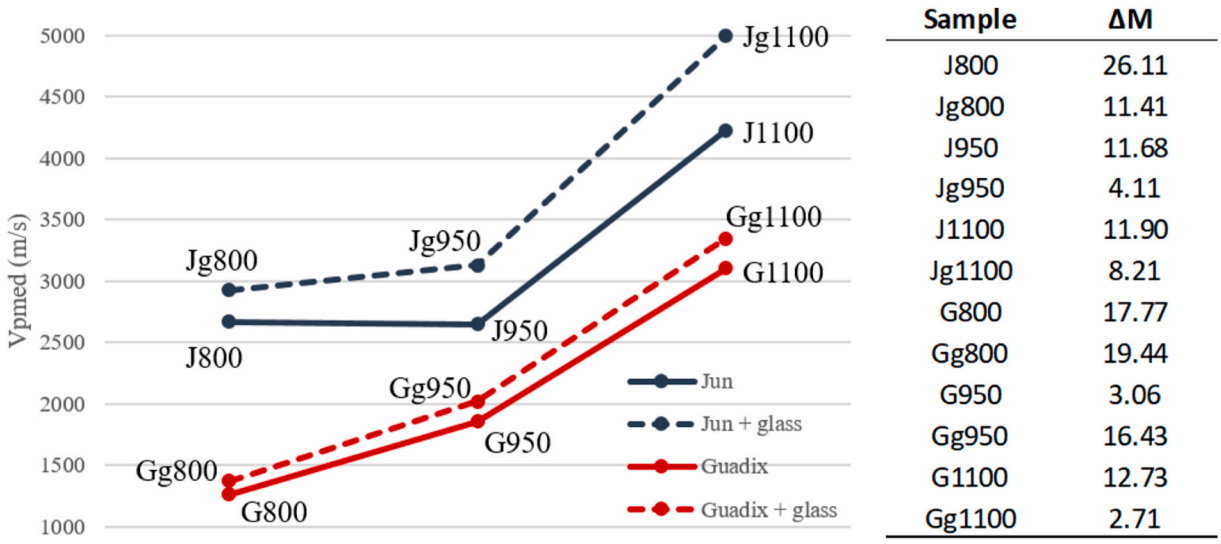

Sample	ΔM
J800	26.11
Jg800	11.41
J950	11.68
Jg950	4.11
J1100	11.90
Jg1100	8.21
G800	17.77
Gg800	19.44
G950	3.06
Gg950	16.43
G1100	12.73
Gg1100	2.71

Fig. 13. Mean ultrasound velocities (in m/s) in fired Jun and Guadix bricks made with and without added glass. The table on the right shows the structural anisotropy (ΔM) of the bricks.

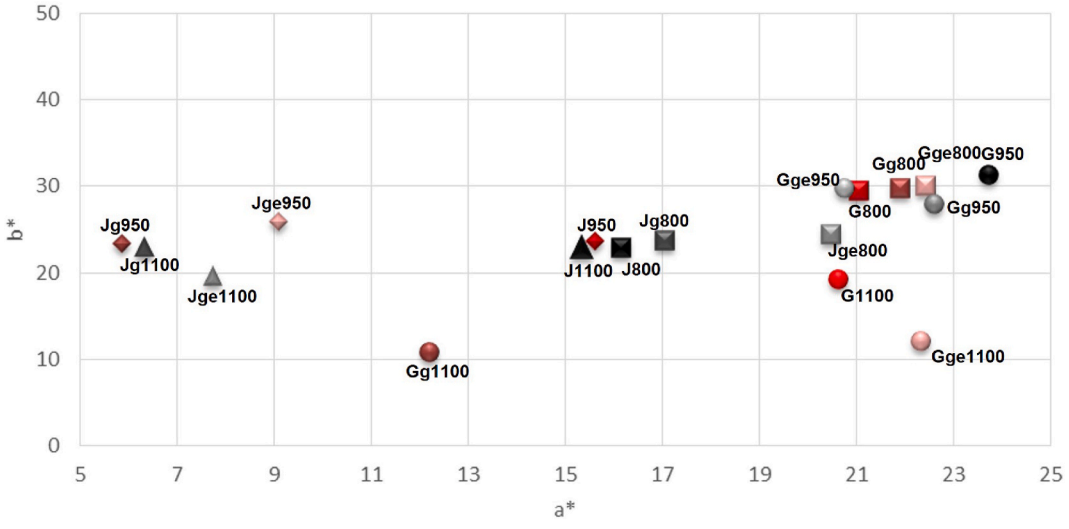

Fig. 14. A) Chromatic values (a* and b*) for handmade and extruded Jun and Guadix bricks with and without added glass.

reduces the decay. The bricks with added glass show less porosity and less water absorption capacity (see Table 4). When comparing the manufacturing processes (handmade or extruded) of the bricks made with glass, the handmade bricks seem to perform better than the extruded ones. This may be due to the different anisotropy (ΔM, Table 6) in that handmade bricks are more homogeneous and therefore more resistant to the crystallization pressures exerted by the water-ice phase change. If we compare the two brick groups, the Guadix bricks fired at 800 °C and the Jun bricks without glass fired at the same temperature suffered the most ice crystallization. In the

Table 6
Lightness (L*), chromatic values (a* and b*), chroma (C*) hue angle (h°) and colour difference (ΔE) values caused by the addition of household glass with respect to the bricks made without additive. Each value indicated is the average of nine values. Standard deviation is indicated in brackets.

	L*	a*	b*	C*	h°	ΔE
J800	58.49 (2.93)	16.13 (0.59)	22.90 (0.79)	28.02 (0.86)	55 (1.03)	1.29
Jg800	59.75 (0.99)	17.03 (0.82)	23.83 (1.60)	29.30 (1.74)	54 (0.89)	
Jge800	61.49 (1.02)	20.46 (0.61)	24.56 (0.84)	28.35 (1.11)	55 (0.95)	
J950	62.96 (1.43)	15.61 (1.15)	23.69 (1.98)	28.38 (2.13)	57 (1.75)	14.39
Jg950	73.55 (2.36)	5.87 (0.89)	23.35 (0.85)	24.10 (0.81)	76 (2.22)	
Jge950	75.62 (0.91)	9.09 (0.29)	25.98 (1.06)	23.47 (1.24)	79 (1.14)	
J1100	62.75 (1.35)	15.35 (1.15)	23.02 (0.72)	27.68 (1.13)	56 (1.60)	9.02
Jg1100	63.01 (1.73)	6.33 (0.97)	22.83 (1.34)	23.72 (1.21)	74 (2.68)	
Jge1100	63.16 (1.41)	7.74 (0.77)	19.55 (1.21)	22.78 (1.04)	72 (1.66)	
G800	55.01 (1.25)	21.04 (0.90)	29.56 (1.24)	36.28 (1.53)	55 (0.24)	1.96
Gg800	53.26 (1.55)	21.88 (0.87)	29.83 (1.15)	36.99 (1.41)	54 (0.45)	
Gge800	52.65 (0.89)	22.41 (0.68)	30.19 (1.13)	36.89 (1.25)	52 (0.30)	
G950	55.18 (2.69)	23.70 (0.97)	31.38 (1.09)	39.33 (1.30)	53 (0.99)	4.77
Gg950	52.01 (2.42)	22.59 (0.92)	28.00 (2.02)	35.99 (1.91)	51 (1.83)	
Gge950	51.82 (2.04)	20.74 (0.61)	29.84 (0.84)	37.12 (1.04)	50 (0.12)	
G1100	44.12 (1.41)	20.61 (1.57)	19.24 (2.05)	28.20 (2.50)	43 (1.26)	11.91
Gg1100	45.14 (1.63)	12.18 (1.89)	10.83 (1.16)	16.31 (1.97)	42 (1.46)	
Gge1100	42.13 (0.97)	22.32 (1.24)	12.14 (1.04)	15.46 (1.46)	43 (1.64)	

Guadix samples, this took the form of a gradual loss of fragments over the course of the test, while in the case of Jun more abrupt jumps were observed (Fig. 15).

3.8.2. Salt crystallization

The handmade and extruded bricks behave differently depending on the type of raw material used and the presence or not of household glass. However, as we observed with the freeze-thaw test, the handmade bricks seem to perform better than the extruded ones. Leshina and Pivnev [13], who used sodium sulphate to simulate freeze-thaw tests, reported that samples containing 20 wt% glass residue were resistant to at least 70 freeze-thaw cycles. The general trend in all the bricks involves an increase in weight at the beginning of the decay test, due to the presence of sodium sulphate in brick pores and fissures, followed by a sharp or more gradual descent in the following cycles (Fig. 16).

The Jun bricks show a rapid weight gain above all at 800 °C until they reach cycle 5, which is when they start to break up and gradually lose fragments. At 950 °C, the bricks generally gain less weight or, as in the case of J950, lose less weight. However, in this case the weight of the brick fluctuates over the 15 cycles. This fluctuation indicates that after the initial crystallization of salts in the pore system (weight gain), these salts start to break the brick down, causing fissures to develop and fragments to fall off (weight loss). Then the salts crystallize again in the new fissures (new weight gain). These weight gains and losses can be observed in various samples over the 15 test cycles. Bricks fired at 1100 °C are more resistant. Resistance also increases when household glass is added, as manifested by the fact that Jg1100 and Jge1100 are the samples that gain least weight and undergo least weight variation. Guadix bricks fired at 800 °C show a smaller weight gain compared to the Jun bricks and a pronounced, constant weight loss just after the second cycle due to powdering. These bricks do not withstand the 15 test cycles and disintegrate before the end of the test (Fig. 16). In a similar way, the Guadix bricks proved more resistant to salt attack as the firing temperature increased and when glass was added (Fig. 16).

3.8.3. Wet-dry

The wet-dry test shows higher weight variations between cycles in the Jun samples than in those from Guadix (Fig. 17). At higher firing temperatures, these variations are reduced due to the sintering and vitrification of the bricks. It should be noted that extruded bricks made with clay from both Jun and Guadix generally undergo higher weight variations than the handmade bricks. This could be due to the fact that the extruded samples retain more moisture within their pore systems than the handmade ones.

4. Conclusions

This paper evaluated how the addition of 20 wt% household glass improves the strength of solid bricks by comparing samples made with two different raw materials (Jun and Guadix), two different manufacturing methods (handmade and extrusion) and three different firing temperatures, 800, 950 and 1100 °C. The clayey soils used as raw materials have different mineralogies. The soil from Jun contains carbonates, while that from Guadix is rich in quartz and phyllosilicates. This leads to differences in the mineralogical evolution of bricks after firing, i.e. the development of new Ca-(Mg-) silicates such as gehlenite, diopside, wollastonite and anorthite when the raw material from Jun was used, while mullite appeared with the raw material from Guadix. The increase in firing temperature also leads to an increase in the amount of amorphous phase due to the vitrification of the bricks. The addition of glass modifies the porous system. In fact, bricks with added household glass fired at high temperature absorb less water and dry more quickly than conventional bricks. It has also been shown that extruded bricks are less porous. The addition of glass leads to a decrease in pore interconnection and augments vitrification. The porosity of both handmade and extruded bricks diminishes as the firing temperature increases.

Bricks with added glass are more resistant to compressive strength tests than those made with just clay. This is more evident in the

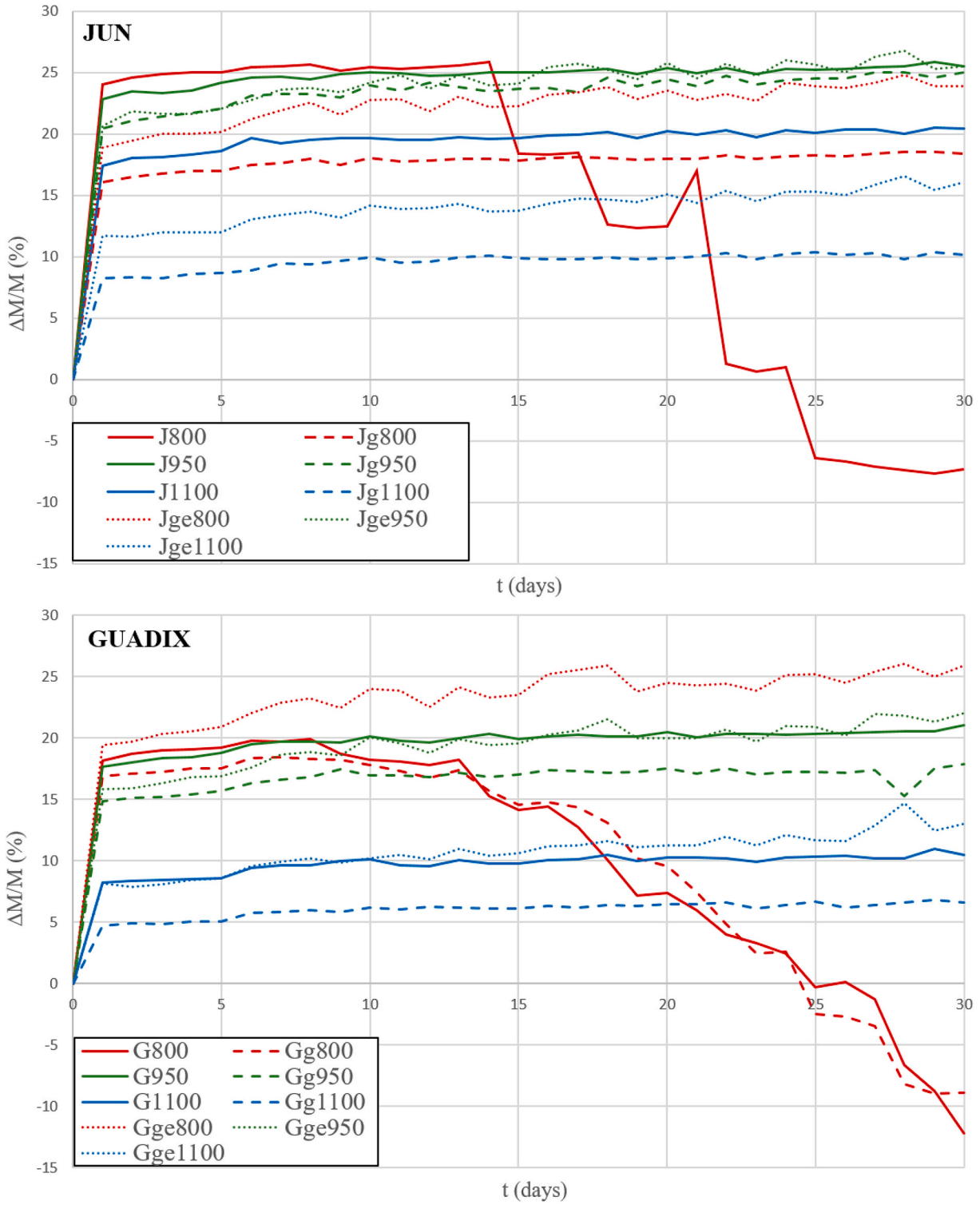

Fig. 15. Freeze-thaw diagrams for handmade and extruded bricks made with clay from Jun or Guadix fired at 800, 950 and 1100 °C with and without the addition of household glass.

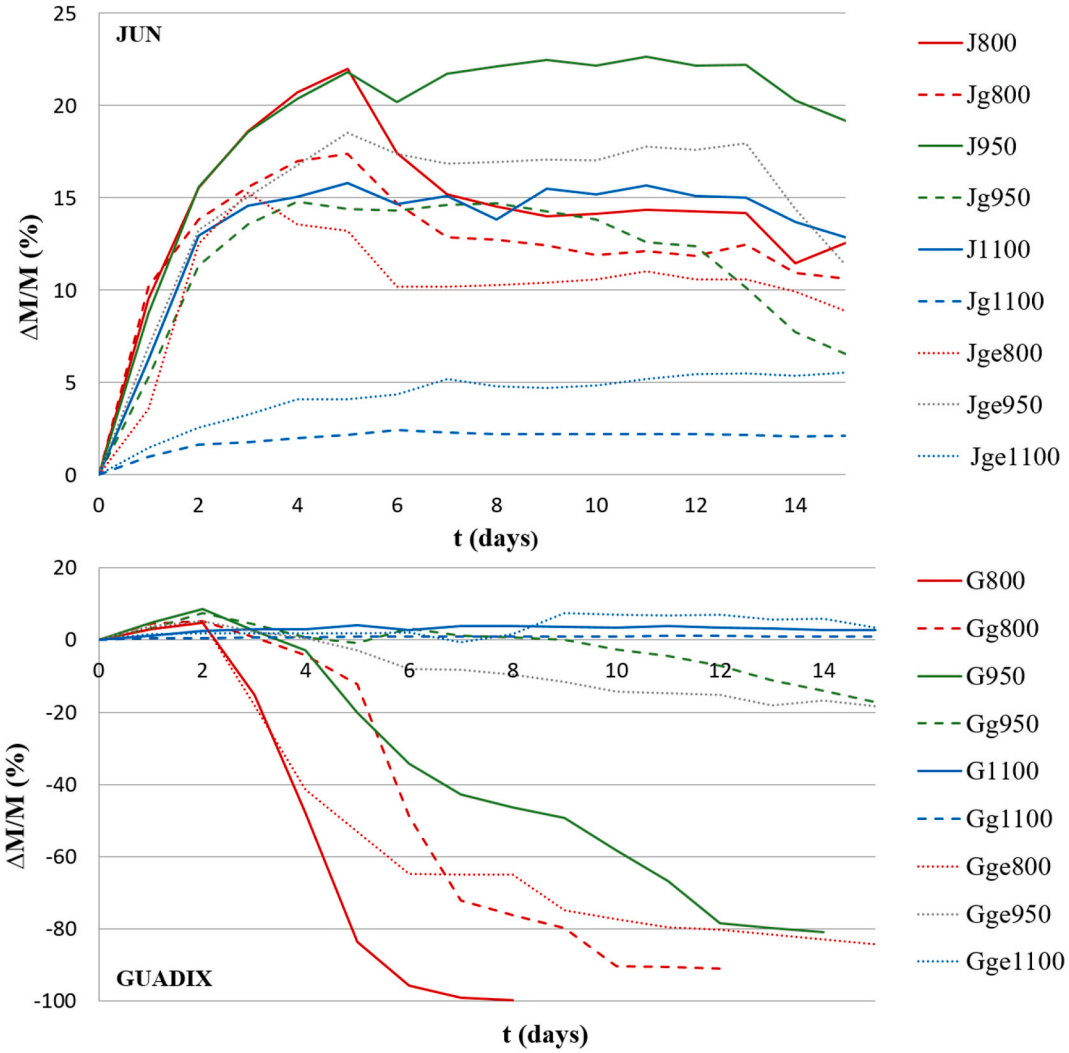

Fig. 16. Salt crystallization diagrams for handmade and extruded bricks made with clay from Jun and Guadix fired at 800, 950 and 1100 °C with and without added household glass.

bricks made with the clay from Jun. These results are confirmed by ultrasound measurements which revealed that the compactness of bricks increases in line with the firing temperature and by adding glass.

The colour of the bricks reflects the composition of the two raw materials (with or without carbonates) and the mineralogical and textural changes that take place during firing. The Jun bricks vary from yellow to orange in colour, while those made with clay from Guadix tend to be dark red. Colour does not seem to be linked with the durability and the physical properties of the bricks.

The Jun bricks perform better than those from Guadix in accelerated ageing tests, perhaps due to the melting action of carbonates at low firing temperatures.

In general, the use of household glass as an additive in the production of bricks provides benefits for the environment and for the brick industry. It also improves certain physical properties of the bricks, for example by making them less porous and reducing their water absorption capacity. It also provides greater resistance and durability. These improvements represent a step forward in the production of more efficient, more environmentally friendly products for use in the construction industry.

Author statement

LCL and GC conceived the research, LCL performed the experiments, LCL and GC analysed the data, LCL wrote the manuscript, GC revised the manuscript.

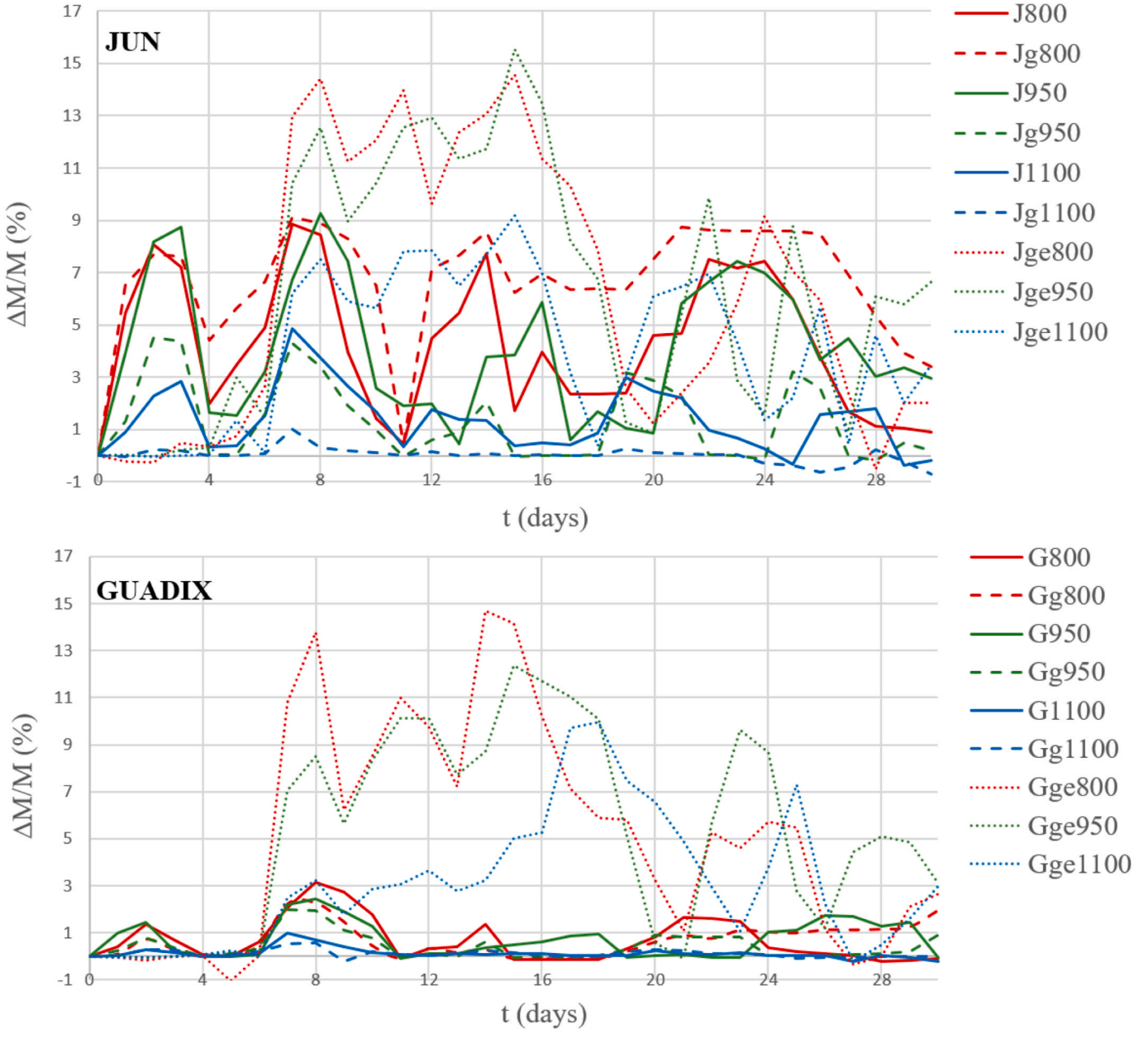

Fig. 17. Wet-dry diagrams of handmade and extruded bricks made with clay from Jun and Guadix fired at 800, 950 and 1100 °C with and without added household glass.

Declaration of competing interest

The authors declare that they have no known competing financial interests or personal relationships that could have appeared to influence the work reported in this paper.

Data availability

Data will be made available on request.

Acknowledgements

This study has been funded by Junta de Andalucía Research Group RNM179 and by Research Projects MAT2016-75889-R and B-RNM-188-UGR20. We are grateful to Nigel Walkington for his assistance in revising the English text of the manuscript and to two anonymous reviewers for their helpful suggestions.

References

[1] R.G. Drysdale, A.A. Hamid, L.R. Baker, Masonry Structures: Behavior and Design, 1994.
[2] J. Bolden, T. Abu-Lebdeh, E. Fini, Utilization of recycled and waste materials in various construction applications, Am. J. Environ. Sci. 9 (1) (2013) 14–24, https://doi.org/10.3844/ajessp.2013.14.24.
[3] R. Dachowski, P. Kostrzewa, The use of waste materials in the construction industry, Procedia Eng. 161 (2016) 754–758, https://doi.org/10.1016/j.proeng.2016.08.764.
[4] N. Sudharsan, K. Sivalingam, Potential utilization of waste material for sustainable development in construction industry, Int. j. recent technol. 8 (3) (2019) 3435–3438, https://doi.org/10.35940/ijrte.C5062.098319.
[5] M. Małek, K. Grzelak, W. Łasica, M. Jackowski, J. Kluczyński, I. Szachogłuchowicz, Torzewski, J. Łuszczek, Cement-glass composite bricks (CGCB) with interior 3D printed PET-G scaffolding, J. Build. Eng. 52 (2022), 104429, https://doi.org/10.1016/j.jobe.2022.104429.
[6] A.A. Gulghane, P.V. Khandve, Management for construction materials and control of construction waste in construction industry: a review, Int. J. Eng. 5 (4) (2015) 59–64.
[7] M. Dabaieh, J. Heinonen, D. El-Mahdy, D.M. Hassan, A comparative study of life cycle carbon emissions and embodied energy between sun-dried bricks and fired clay bricks, J. Clean. Prod. 275 (2020), 122998, https://doi.org/10.1016/j.jclepro.2020.122998.
[8] D.H. Vu, K.S. Wang, J.H. Chen, B.X. Nam, B.H. Bac, Glass–ceramic from mixtures of bottom ash and fly ash, J. Waste Manag 32 (12) (2012) 2306–2314, https://doi.org/10.1016/j.wasman.2012.05.040.
[9] F. Trotti, P. Mozzo, A. Temporin, M. Lanciai, F. Predicatori, F. Righetti, A. Tacconi, CR-39 track detectors applied to measurements of 210Po embedded in household glass, Environ. Int. 22 (1996) 863–869, https://doi.org/10.1016/S0160-4120(96)00194-8.
[10] S.N. Monteiro, C.M.F. Vieira, On the production of fired clay bricks from waste materials: a critical update, Construct. Build. Mater. 68 (2014) 599–610, https://doi.org/10.1016/j.conbuildmat.2014.07.006.
[11] P. Chindaprasirt, A. Srisuwan, C. Saengthong, S. Lawanwadeekul, N. Phonphuak, Synergistic effect of fly ash and glass cullet additive on properties of fire clay bricks, J. Build. Eng. 44 (2021), 102942, https://doi.org/10.1016/j.jobe.2021.102942.
[12] S. Palaniyappan, V.E. Annamalai, S. Ashwinkumaran, D. Thenmuhil, D. Veeman, Utilization of abrasive industry waste as a substitute material for the production of fireclay brick, J. Build. Eng. 45 (2022), 103606, https://doi.org/10.1016/j.jobe.2021.103606.
[13] V.A. Leshina, A.L. Pivnev, Ceramic wall materials using glass waste, Glass Ceram. 59 (2002) 356–358, https://doi.org/10.1023/A:1022090814669.
[14] D. Whitehouse, Glass: a Short History, Smithsonian Inst Press, 2012 [15] Gusain, G. S., Rautela, B. S., Ramola, R. C., 2012. Estimation of past radon exposure to indoor radon from embedded Po210 in household glass. Radiat. Prot. Dosim., 152(1-3), 46-50. https://doi.org/10.1093/rpd/ncs149.
[15] F.C. Trevelyan, R.A. Haslam, Musculoskeletal disorders in a handmade brick manufacturing plant, J. Ind. Ergon. 27 (1) (2001) 43–55, https://doi.org/10.1016/S0169-8141(00)00036-6.
[16] K.L. Lin, L.S. Huang, J.L. Shie, C.J. Cheng, C.H. Lee, T.C. Chang, Elucidating the effects of solar panel waste glass substitution on the physical and mechanical characteristics of clay bricks, Environ. Technol. 34 (1) (2013) 15–24, https://doi.org/10.1080/09593330.2012.679693.
[17] M.E. Tyrrell, A.H. Goode, Waste Glass as a Flux for Brick Clays, vol. 7701, US Department of Interior, Bureau of Mines, 1972.
[18] M.E. Tyrrell, I.L. Feld, J.A. Barclay, Fabrication and Cost Evaluation of Experimental Building Brick from Waste Glass, vol. 7605, US Department of Interior, Bureau of Mines, 1972.
[19] V. Loryuenyong, T. Panyachai, K. Kaewsimork, C. Siritai, Effects of recycled glass substitution on the physical and mechanical properties of clay bricks, J. Waste Manag. 29 (10) (2009) 2717–2721, https://doi.org/10.1016/j.wasman.2009.05.015.
[20] S.M. Kazmi, S. Abbas, M.L. Nehdi, M.A. Saleem, M.J. Munir, Feasibility of using waste glass sludge in production of ecofriendly clay bricks, J. Mater. Civ. Eng. 29 (8) (2017), 04017056, https://doi.org/10.1061/(ASCE)MT.1943-5533.0001928.
[21] N. Saenz, E. Sebastián, G. Cultrone, Analysis of tempered bricks: from raw material and additives to fired bricks for use in construction and heritage conservation, Eur. J. Mineral 31 (2) (2019) 301–312, https://doi.org/10.1127/ejm/2019/0031-2832.
[22] M. Hasan, A. Siddika, M. Akanda, P. Ali, M. Islam, Effects of waste glass addition on the physical and mechanical properties of brick, Innovative Infrastructure Solutions 6 (1) (2021) 1–13, https://doi.org/10.1007/s41062-020-00401-z.
[23] L. Mao, Y. Wu, W. Zhang, Q. Huang, The reuse of waste glass for enhancement of heavy metals immobilization during the introduction of galvanized sludge in brick manufacturing, J. Environ. Manag. 231 (2019) 780–787.
[24] L. Mao, H. Zhou, M. Peng, L. Hu, W. Zhang, Effects of waste glass particle size on improving the property and environmental safety of fired brick containing electroplating sludge, Construct. Build. Mater. 257 (2020), 119583, https://doi.org/10.1016/j.conbuildmat.2020.119583.
[25] C. Viseras, Estratigrafía y sedimentología del relleno aluvial de la Cuenca de Guadix (Cordilleras Béticas), Ph.D. Thesis, Universidad de Granada, 1991, p. 327.
[26] J.M. García-Aguilar, J.M. Martín, Late Neogene to recent continental history and evolution of the Guadix-Baza Basin (SE Spain), Rev. Soc. Geol. 13 (2000) 65–77.
[27] A. García-Alix, R. Minwer-Barakat, J.M. Martín, E. Martín-Suárez, M. Freudenthal, Biostratigraphy and sedimentary evolution of late Miocene and Pliocene continental deposits of the Granada Basin (southern Spain), Lethaia 41 (2008) 431–446, https://doi.org/10.1111/j.1502-3931.2008.00097.x.
[28] M. Dondi, G. Guarini, M. Raimondo, C. Zanelli, Recycling PC and TV waste glass in clay bricks and roof tiles, J. Waste Manag. 29 (6) (2009) 1945–1951, https://doi.org/10.1016/j.wasman.2008.12.003.
[29] N. Phonphuak, S. Kanyakam, P. Chindaprasirt, Utilization of waste glass to enhance physical–mechanical properties of fired clay brick, J. Clean. Prod. 112 (2016) 3057–3062, https://doi.org/10.1016/j.jclepro.2015.10.084.
[30] R.T. Laird, M. Worcester, The inhibiting of lime blowing, Transactions of the Br. Ceram. Trans. 55 (1956) 545–563.
[31] D.M. Moore, R.C. Reynolds Jr., X-ray Diffraction and the Identification and Analysis of Clay Minerals, Oxford University Press (OUP), 1989.
[32] UNE-EN 13755, Métodos de ensayo para piedra natural. Determinación de la absorción de agua a presión atmosférica, AENOR, Madrid, 2008.
[33] NORMAL 29/88, Misura dell'indice di asciugamento (drying index), CNR-ICR, Roma, Italia, 1988.
[34] UNE-EN 1925, Métodos de ensayo para piedra natural. Determinación de la resistencia a la compresión uniaxial, AENOR, Madrid, 1999.

[35] G. Cultrone, M.J. De La Torre, E. Sebastián, O. Cazalla, Evaluation of bricks durability using destructive and non destructive methods (DT and NDT), Mater. Constr. 53 (269) (2003) 41–60, https://doi.org/10.3989/mc.2003.v53.i269.267.
[36] RILEM, Recommended tests to measure the deterioration of stone and to assess the effectiveness of treatment methods. Commision 25-PEM: Protection et Erosion des Monuments, Mater. Struct. 13 (75) (1980) 175–253.
[37] UNE-EN 1926, Métodos de ensayo para piedra natural. Determinación del coeficiente de absorción de agua por capilaridad, AENOR, Madrid, 2007.
[38] ASTM D2845, Standard Test Method for Laboratory Determination of Pulse Velocities and Ultrasonic Elastic Constants of Rock, J. ASTM Int., West Conshohocken, PA, USA, 2000.
[39] J. Guyader, A. Denis, Propagation des ondes dans les roches anisotropes sous contrainte évaluation de la qualité des schistes ardoisiers, Bulletin of the International Association of Engineering Geology-Bulletin de l'Association Internationale de Géologie de l'Ingénieur 33 (1) (1986) 49–55, https://doi.org/10.1007/BF02594705.
[40] UNE-EN 15886, Métodos de ensayo. Medición del color de superficies, AENOR, Madrid, 2011.
[41] UNE-EN 12371, Métodos de ensayo para piedra natural. Determinación de la resistencia a la heladicidad, AENOR, Madrid, 2011.
[42] UNE-EN 12370, Métodos de ensayo para piedra natural. Determinación de la resistencia a la cristalización de sales, AENOR, Madrid, 2002.
[43] D.5313 Astm, Standard Test Method for Evaluation of Durability of Rock for Erosion Control under Wetting and Drying Conditions, J. ASTM Int, West Conshohocken, PA, USA, 2004.
[44] Y. Maniatis, M.S. Tite, Technological examination of neolithic-bronze age pottery from central and southeast Europe and from the near East, J. Archaeol. Sci. 8 (1) (1981) 59–76, https://doi.org/10.1016/0305-4403(81)90012-1.
[45] C.N. Djangang, E. Kamseu, A. Elimbi, G.L. Lecomte, P. Blanchart, Net-shape clay ceramics with glass waste additive, Int. J. Mater. Sci. Appl. 5 (8) (2014) 592–602, https://doi.org/10.4236/msa.2014.58061.
[46] E. Tiffo, A. Elimbi, J.D. Manga, A.B. Tchamba, Red ceramics produced from mixtures of kaolinite clay and waste glass, Braz. J. Sci. 2 (1) (2015) 1–13, https://doi.org/10.1186/s40552-015-0009-9.
[47] S.E. Chidiac, L.M. Federico, Effects of waste glass additions on the properties and durability of fired clay brick, Can. J. Civ. 34 (11) (2007) 1458–1466, https://doi.org/10.1139/L07-120.
[48] G. Cultrone, Estudio mineralógico-petrográfico y físico-mecánico de ladrillos macizos para su aplicación en intervenciones del patrimonio histórico, Doctoral dissertation, Universidad de Granada, 2001, p. 292.
[49] D.L. Whitney, B.W. Evans, Abbreviations for names of rock-forming minerals, Am. Mineral. 95 (2010) 185–187, https://doi.org/10.2138/am.2010.3371.
[50] C.M.F. Vieira, R. Sánchez, S.N. Monteiro, Characteristics of clays and properties of building ceramics in the state of Rio de Janeiro, Brazil, Construct. Build. Mater. 22 (5) (2008) 781–787, https://doi.org/10.1016/j.conbuildmat.2007.01.006.
[51] F. Guo, F. Wu, Y. Mu, Y. Hu, X. Zhao, W. Meng, Y. Lin, Characterization of organic matter of plants from lakes by thermal analysis in a N_2 atmosphere, Sci. Rep. 6 (1) (2016) 1–7, https://doi.org/10.1038/srep22877.
[52] G.W. Brindley, M. Nakahira, The kaolinite-mullite reaction series: I, a survey of outstanding problems, J. Am. Ceram. Soc. 42 (7) (1959) 311–314, https://doi.org/10.1111/j.1151-2916.1959.tb14314.x.
[53] J.P. Eberhart, Etude des transformations du mica muscovite par chauffage entre 700 et 1200 C, Bull. Mineral. 86 (3) (1963) 213–251, https://doi.org/10.3406/bulmi.1963.5644.
[54] S.G. Barlow, D.A.C. Manning, Influence of time and temperature on reactions and transformations of muscovite mica, Br. Ceram. Trans. 98 (3) (1999) 122–126, https://doi.org/10.1179/096797899680327.
[55] B. Velde, Upper stability of muscovite, Am. Mineral. 51 (5–6) (1966) 924–929.
[56] C. Rodriguez-Navarro, G. Cultrone, A. Sanchez-Navas, E. Sebastian, TEM study of mullite growth after muscovite breakdown, Am. Mineral. 88 (5–6) (2003) 713–724, https://doi.org/10.2138/am-2003-5-601.
[57] A. Sanchez-Navas, Sequential kinetics of a muscovite-out reaction: a natural example, Am. Mineral. 84 (9) (1999) 1270–1286, https://doi.org/10.2138/am-1999-0905.
[58] G. Cultrone, I. Aurrekoetxea, C. Casado, A. Arizzi, Sawdust recycling in the production of lightweight bricks: how the amount of additive and the firing temperature influence the physical properties of the bricks, Construct. Build. Mater. 235 (2020), 117436, https://doi.org/10.1016/j.conbuildmat.2019.117436.
[59] D. Eliche-Quesada, M.A. Felipe-Sesé, J.A. López-Pérez, A. Infantes-Molina, Characterization and evaluation of rice husk ash and wood ash in sustainable clay matrix bricks, Ceram. Int. 43 (1) (2017) 463–475, https://doi.org/10.1016/j.ceramint.2016.09.181.
[60] C. Rodriguez-Navarro, E. Ruiz-Agudo, A. Luque, A.B. Rodriguez-Navarro, M. Ortega-Huertas, Thermal decomposition of calcite: mechanisms of formation and textural evolution of CaO nanocrystals, Am. Mineral. 94 (4) (2009) 578–593, https://doi.org/10.2138/am.2009.3021.
[61] C. Rodríguez Navarro, K. Kudlacz, E. Ruiz Agudo, The mechanism of thermal decomposition of dolomite: new insights from 2D-XRD and TEM analyses, Am. Mineral. 97 (1) (2012) 38–51, https://doi.org/10.2138/am.2011.3813.
[62] J. Parras, C. Sánchez-Jimeñez, M. Rodas, F.J. Luque, Ceramic applications of middle ordovician shales from central Spain, Appl. Clay Sci. 11 (1) (1996) 25–41, https://doi.org/10.1016/0169-1317(96)00003-8.
[63] C. Rathossi, Y. Pontikes, Effect of firing temperature and atmosphere on ceramics made of NW Peloponnese clay sediments. Part I: reaction paths, crystalline phases, microstructure and colour, J. Eur. Ceram. Soc. 30 (9) (2010) 1841–1851, https://doi.org/10.1016/j.jeurceramsoc.2010.02.002.
[64] G. Cultrone, F.J.C. Rosua, Growth of metastable phases during brick firing: mineralogical and microtextural changes induced by the composition of the raw material and the presence of additives, Appl. Clay Sci. 185 (2020), 105419, https://doi.org/10.1016/j.clay.2019.105419.
[65] J. Capel, F. Huertas, J. Linares, High temperature reactions and use of bronze age pottery from La Mancha, central Spain, Mineral. Petrogr. Acta 29 (1985) 563–575.
[66] C. Rodriguez-Navarro, G. Cultrone, A. Sanchez-Navas, E. Sebastian, TEM study of mullite growth after muscovite breakdown, Am. Mineral. 88 (5–6) (2003) 713–724, https://doi.org/10.2138/am-2003-5-601.
[67] A. De Bonis, G. Cultrone, C. Grifa, A. Langella, A.P. Leone, M. Mercurio, V. Morra, Different shades of red: the complexity of mineralogical and physico-chemical factors influencing the colour of ceramics, Ceram. Int. 43 (11) (2017) 8065–8074, https://doi.org/10.1016/j.ceramint.2017.03.127.
[68] C. Coletti, L. Maritan, G. Cultrone, M.C. Dalconi, A. Hein, E. Molina, C. Mazzoli, Recycling trachyte waste from the quarry to the brick industry: effects on physical and mechanical properties, and durability of new bricks, Construct. Build. Mater. 166 (2018) 792–807, https://doi.org/10.1016/j.conbuildmat.2018.01.158.
[69] S. Vichaphund, M. Kitiwan, D. Atong, P. Thavorniti, Microwave synthesis of wollastonite powder from eggshells, J. Eur. Ceram. Soc. 31 (14) (2011) 2435–2440, https://doi.org/10.1016/j.jeurceramsoc.2011.02.026.
[70] H. Wang, Q. Zhang, H. Yang, H. Sun, Synthesis and microwave dielectric properties of CaSiO3 nanopowder by the sol–gel process, Ceram. Int. 34 (6) (2008) 1405–1408, https://doi.org/10.1016/j.ceramint.2007.05.001.
[71] P. Saravanapavan, L.L. Hench, Mesoporous calcium silicate glasses. I. Synthesis, J. Non-Cryst. Solids 318 (1–2) (2003) 1–13, https://doi.org/10.1016/S0022-3093(02)01864-1.
[72] G. Cultrone, E. Sebastián, K. Elert, M.J. De la Torre, O. Cazalla, C. Rodriguez–Navarro, Influence of mineralogy and firing temperature on the porosity of bricks, J. Eur. Ceram. Soc. 24 (3) (2004) 547–564, https://doi.org/10.1016/S0955-2219(03)00249-8.
[73] K. Elert, G. Cultrone, C.R. Navarro, E.S. Pardo, Durability of bricks used in the conservation of historic buildings—influence of composition and microstructure, J. Cult. Herit. 4 (2) (2003) 91–99, https://doi.org/10.1016/S1296-2074(03)00020-7.
[74] M.S. Tite, Y. Maniatis, Scanning electron microscope of fired calcareous clays, Br. Ceram. Trans., No. 74 (1975) 19–22.
[75] R.L.-88 Pliego, Pliego General de Condiciones para la Recepción de Ladrillos Cerámicos en las Obras de Construcción, Ministerio de Obras Públicas, Transportes y Medio Ambiente, Spain, 1988.
[76] J. Martínez-Martínez, D. Benavente, M.G. Del Cura, Petrographic quantification of brecciated rocks by image analysis. Application to the interpretation of elastic wave velocities, Eng. Geol. 90 (1–2) (2007) 41–54, https://doi.org/10.1016/j.enggeo.2006.12.002.

[77] J.M. Martínez, D. Benavente, M.G. del Cura, Spatial attenuation: th e most sensitive ultrasonic parameter for detecting petrographic features and deca y processes in carbonatic rocks, Eng. Geol. 119 (2011) 84–95, https://doi.org/10.1016/j.enggeo.2011.02.002.
[78] P. Chindaprasirt, A. Srisuwan, C. Saengthong, S. Lawanwadeekul, N. Phonphuak, Synergistic effect of fly ash and glass cullet additive on properties of fire clay bricks, J. Build. Eng. 44 (2021), 102942, https://doi.org/10.1016/j.jobe.2021.102942.
[79] J.M. Alia, H.G.M. Edwards, F.J. Garcia-Navarro, J. Parras-Armenteros, C.J. Sanchez-Jimenez, Application of FT-Raman spectroscopy to quality control in brick clays firing process, Talanta 50 (2) (1999) 291–298, https://doi.org/10.1016/S0039-9140(99)00031-4.
[80] L. Nodari, E. Marcuz, L. Maritan, C. Mazzoli, U. Russo, Hematite nucleation and growth in the firing of carbonate-rich clay for pottery production, J. Am. Ceram. Soc. 27 (16) (2007) 4665–4673, https://doi.org/10.1016/j.jeurceramsoc.2007.03.031.
[81] C.M. Grossi, P. Brimblecombe, R.M. Esbert, F.J. Alonso, Colour changes in architectural limestones from pollution and cleaning, Color Res. Appl. 32 (2007) 320–331, https://doi.org/10.1002/col.20322.